Russian Geology and Geophysics © 2019, V.S. Sobolev IGM, Siberian Branch of the RAS
Vol. 60, No. 8, pp. 890–910, 2019 *DOI:10.15372/RGG2019057* *Geologiya i Geofizika*

Stages and Duration of Formation of the Kalguty Mo–W Ore-Magmatic System (Altai): Thermochronology and Mathematical Modeling

A.G. Vladimirov [a,b,c,] ✉, I.Yu. Annikova [a,b], N.G. Murzintsev [a], A.V. Travin [a,b,c], E.N. Sokolova [a,b], S.Z. Smirnov [a,b,c], O.A. Gavryushkina [a,b], T.A. Oitseva [d]

[a] *V.S. Sobolev Institute of Geology and Mineralogy, Siberian Branch of the Russian Academy of Sciences, pr. Akademika Koptyuga 3, Novosibirsk, 630090, Russia*

[b] *Novosibirsk State University, ul. Pirogova 2, Novosibirsk, 630090, Russia*

[c] *Tomsk State University, pr. Lenina 36, Tomsk, 634050, Russia*

[d] *East Kazakhstan State Technical University, ul. Protozanova 69, Ust'-Kamenogorsk, 070004, Republic of Kazakhstan*

Received 20 February 2018; received in revised form 29 October 2018; accepted 8 November 2018

Abstract—The Kalguty Mo–W ore-magmatic system (OMS) is a granite batholith ($S = 70$ km^2, $V = 12{,}800$ km^3 at the recent denudation level, according to geological and geophysical data). This batholith is cut by the East Kalguty belt of rare-metal ongonite–elvan dikes spatially and temporally associated with the East Kalguty quartz-vein–greisen Mo–W deposit. Geological and petrogenetic studies along with published and our new results of geochronological (U/Pb zircon, Re/Os molybdenite, and $^{40}Ar/^{39}Ar$ biotite and muscovite) dating made it possible to reconstruct the thermochronological history of the Kalguty OMS. Five stages have been recognized: I (215 ± 1 Ma)—formation of granites of major intrusive phase and of Mo-rich mineralization, which is an orebody called the Molybdenum stock; II (206 ± 1 Ma)—formation of leucogranite and intragranitic-pegmatite stocks in the granites of major intrusive phase; III (202 ± 1 Ma)—formation of most of ongonite–elvan dikes composing a dike belt; IV (195 ± 1 Ma)—formation of long ultrarare-metal ongonite–elvan dikes in the central part of the dike belt, which is spatially associated with the W-rich veins of the deposit; and V (181 ± 1 Ma)—formation of thin ongonite–elvan dikes on the periphery of the dike belt. The recognized age stages of the Kalguty Mo–W ore-magmatic system were mathematically tested based on the model of crystallization differentiation and the dynamics of heat and mass transfer in the magma chamber corresponding to the Kalguty granite batholith. The results obtained show that the formation of a granite batholith (215 ± 1 Ma) and a later ongonite–elvan dike complex with Mo–W-rich mineralization (195 ± 1 Ma) can be explained only by a two-level ore-magmatic system with the "upper" granite batholith at a depth of 5–15 km and the "lower" granite chamber at a depth of 20–31 km. The total duration of ore-magmatic processes is 20 Myr (ore production stage) or 30 Myr, if we take into account occasional elvan dikes with poor quartz–fluorite–barite–ferberite mineralization (181 ± 1 Ma) on the periphery of the Kalguty deposit.

Keywords: rare-metal granites, ongonites, elvans, Mo–W deposits, U/Pb and Ar/Ar isotope dating, thermochronology, mathematical modeling, Gorny Altai

INTRODUCTION

Estimation of the duration of formation of rare-metal–granite ore-magmatic systems (OMS), including that with the participation of granitoid batholiths, ongonites, and elvans, is paid little attention in the scientific literature. There is a common belief based on experimental data and mathematical modeling that silicic magma cannot be in the molten state for a long time. In particular, rare-metal–granite melt solidifies for hundreds of thousands–few millions of years depending on the volume of a magma chamber (Averkin et al., 1988; Sharapov and Averkin, 1990; Vladimirov et al., 1993; Kovalenko et al., 1999). These concepts are confirmed by isotope-geochronological data on ore-magmatic systems corresponding to hypabyssal facies (e.g., Li–F granites of eastern Transbaikalia (Kostitsyn et al., 2004)). The ages of these systems are close to the temporal stages of the origin and extinction of ore-bearing hydrothermal systems (≤0.5–2.0 Ma) (Merceron et al., 1992).

At the same time, most of publications present only results of isotope dating of igneous rocks, while the age of ore objects (intramagmatic and/or postmagmatic mineralization) is established from geological observations and corresponding geochemical signatures of granites: Beauvoir rare-metal granites (France) (Raimbault et al., 1995), granite complexes with ongonites and Sn–W mineralization of the Chukchi Peninsula and Amur region (Alekseev, 2013), Khangilai rare-metal ore belt in eastern Transbaikalia, including the Orlovka (Ta–Nb) and Spokoinoe (W) deposits (Kovalenko et al., 1999; Badanina et al., 2010), topaz–protolithionite granites and ongonites of the Bazardara ore dis-

✉ Corresponding author.
E-mail adress: Vladimir@igm.nsc.ru (A.G. Vladimirov)

trict (southeastern Pamir) (Vladimirov et al., 1991), and Sn-bearing granite–leucogranites of the Piaoak Massif (North Vietnam) (Vladimirov et al., 2012b). Analysis of these data shows the existence of short-term ore-magmatic pulses (magma chamber => magmatic-melt differentiation => ore-bearing hydrothermal fluids) typical of granitoid plutons and associated hydrothermal systems at the hypabyssal level (0.5–2.0 kbar, h = 1.5–7.0 km).

With depth (mesoabyssal and abyssal facies, $h \geq 10$–15 km), the duration of the formation of ore-magmatic systems significantly exceeds the common model estimates. For example, long intervals of formation (tens of millions of years) were established for some granitoid batholiths associated with rare-metal mineralization: granites of the Asian tin belt (Cobbing et al., 1986), Cornubian batholith (Darbyshire and Shepherd, 1994), Erzgebirge Mountains in the Czech Republic (Štemprok et al., 2005), Voznesenka OMS in Primorye (Gonevchuk, 2002; Rub and Rub, 2006), and rare-metal granites and spodumene pegmatites of the Kalba–Narym ore zone (East Kazakhstan) (D'yachkov, 2012; Vladimirov et al., 2012a; Oitseva et al., 2016) and Transbaikalia (Zagorsky et al., 2014; Antipin et al., 2016).

In this paper we make the first attempt to solve this problem. We apply two independent approaches to the estimation of the duration of formation of rare-metal ore-magmatic systems including granitoid batholiths and postgranite ongonite–elvan dikes. The first approach implies a thermochronological analysis of geologic objects, using U/Pb and $^{40}Ar/^{39}Ar$ isotope dating (Travin, 2016). The second approach is mathematical testing of the established age boundaries, based on the model of crystallization differentiation and the dynamics of heat and mass transfer in a magma chamber corresponding to a granitoid batholith (Murzintsev et al., 2016).

The Kalguty granitoid batholith and the Kalguty Mo–W deposit (Gorny Altai) were chosen as an object of research. We comprehensively studied rocks and ores of all stages of formation of rare-metal OMS (granites, leucogranites, intragranitic pegmatites and stockworks, postgranite dikes, and Mo–W quartz–ore veins and greisens) within one denudation level and obtained reliable geological and geophysical data on the deep morphology and structure of the granite batholith (Annikova et al., 2004).

GEOLOGICAL ESSAY

Tectonic setting. The Kalguty OMS is an example of the relationship between granite magmatism and rare-metal–Mo–W mineralization. It formed at the intraplate stage related to the tectonomagmatic activity and, hence, intense shear–pull-apart dislocations of the lithosphere in the Altai accretion–collision orogen under the impact of the Siberian superplume (Dobretsov et al., 2005; Vladimirov et al., 2005). A number of ore-magmatic systems formed in this geodynamic setting; among them are large and unique deposits of Mo, W, Sn, Li, Rb, Cs, Ta, Nb, and Be (Shcherba et al., 1998, 2000; Vladimirov et al., 2003, 2012a; Dobretsov et al., 2010; Kuz'min and Yarmolyuk, 2011; D'yachkov, 2012). The Kalguty OMS should be considered an autonomous magma chamber area in the geologic structures of the Altai accretion–collision system (Figs. 1 and 2). It is genetically related to a deep-seated magma chamber, a granite batholith (S = 70 km^2, V = 12,800 km^3 at the recent denudation level, according to geological and geophysical data (Annikova et al., 2004)). The batholith is cut by ongonite–elvan dikes spatially and temporally associated with the Kalguty quartz-vein–greisen Mo–W deposit. Geological, petrographic, and mineralogical characteristics of the igneous complexes and ore objects of the Kalguty OMS are given elsewhere (Dergachev et al., 1981; Dergachev, 1988, 1989a,b; Vladimirov et al., 1997, 1998; Titov et al., 2001; Annikova et al., 2006; Potseluev et al., 2008; Sokolova et al., 2011a; Gusev, 2011). Here we note the main features of this ore-magmatic system, which are necessary for the correct assessment of the duration of its formation.

Deep morphology of the Kalguty granitoid batholith was determined from gravity field maps of the Kalguty region: map of residual gravity anomalies ($Dg_{res} = Dg_{obs} - Dg_h = 10$ km) of scale 1:200,000, regional-background map of scale 1:500,000 (Dg_h = 10 km), and isodynamic-line maps of scale 1:50,000. Model calculations were made based on Dg_{obs} obtained by summing the values of the regional background and residual anomalies. Modeling of gravity and magnetic anomalies is based on an integrated approach to the interpretation of gravimetry, magnetometry, seismic-survey, and geological data (Vasilevskii, 1980; Vitte, 1981; Vitte and Vasilevsky, 1988). Modeling of gravity anomalies along major profiles (Fig. 3) yielded the following results (Annikova et al., 2004):

(1) A 1–2 km wide "stem" stretching in the NE direction and dipping to the SE at 45–60º was revealed in the central part of the batholith.

(2) Northeast of the central part of the batholith and the deeply underlying "stem", granites compose a 6–9 km thick bed-like body steeply scarping at the boundary of the Kalguty volcanoplutonic structure.

(3) Southeast of the central part of the batholith and the deeply underlying "stem", granites compose a body of intricate shape, which can be interpreted as a series of blocks steeply dipping to the SE, with a strong decrease in the granite thickness to 3–4 km.

Igneous complexes of the Kalguty OMS include the Kalguty pluton of porphyritic rare-metal granites of major phase (Fig. 2), intrusive leucogranite stocks (Argamdzhi, Dzhumala, and Eastern), and the East Kalguty ongonite–elvan dike belt (Fig. 4). The major-phase rocks are biotite and coarse-grained porphyritic two-mica granites of the mesoabyssal facies.

A special mapping performed by Dergachev (1988, 1989a) within the 10–15 km long and ~3 km wide East Kalguty dike belt revealed 125 ongonite and elvan dikes tens of

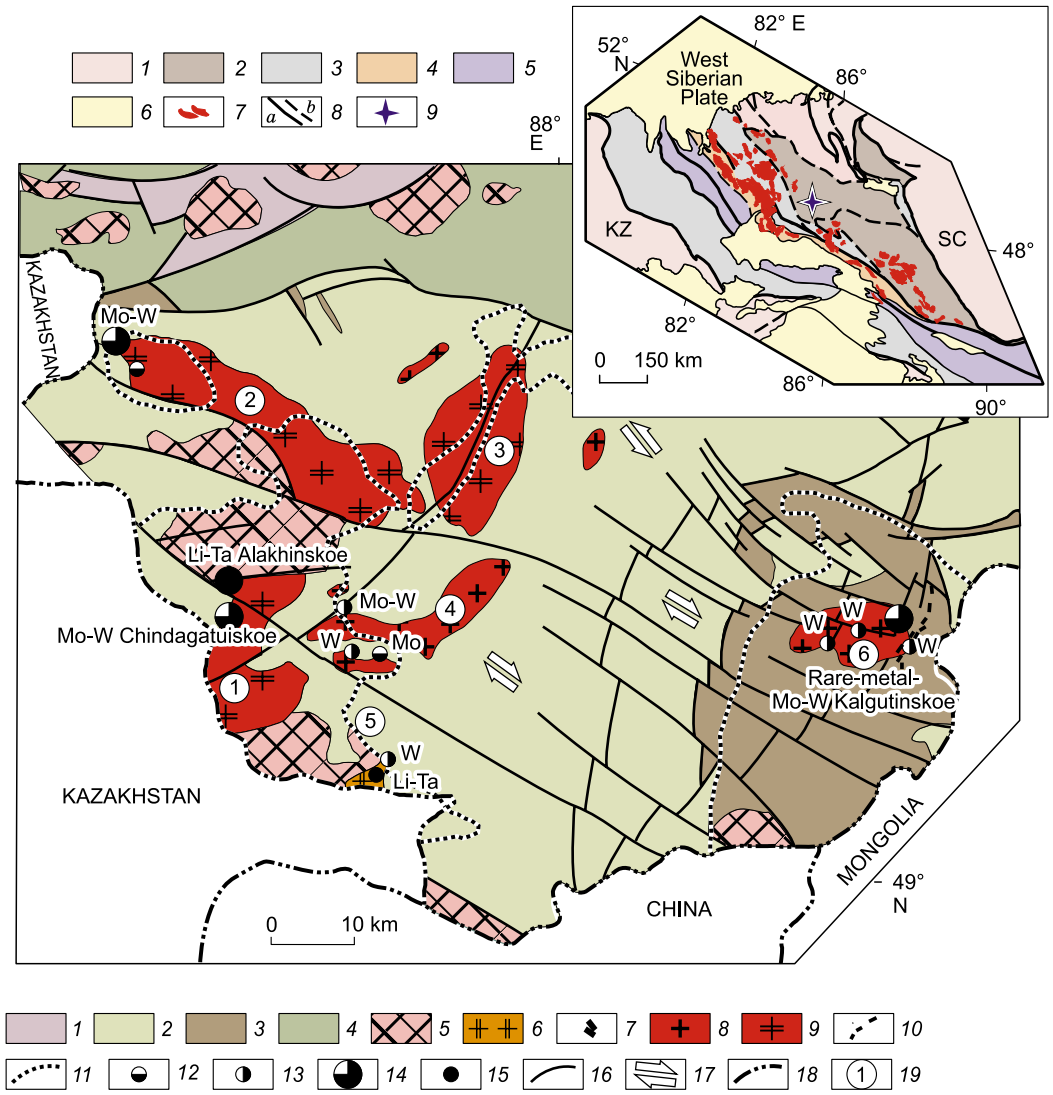

Fig. 1. Schematic map of the location of Late Paleozoic–Early Mesozoic granitoid batholiths and rare-metal deposits in the geologic structures of southern Gorny Altai, after Vladimirov et al. (1997, 2003), Shokal'skii et al. (2000), and Annikova et al. (2006), modified. *1*, structure-lithologic complexes of the Vendian–Early Cambrian accretionary prism in Gorny Altai; *2–4*, Kholzun–Chuya terrane within the Altai–Mongolian microcontinent: *2*, lower structural stage, Early Paleozoic turbidite strata, *3*, upper structural stage, Middle Paleozoic volcanosedimentary strata, *4*, collisional suture, South Chuya metamorphic complex (PZ_1–PZ_2); *5*, Middle Paleozoic collisional granitoids having a calc-alkalic composition within the Kholzun–Chuya terrane and a monzonitoid composition within the South Chuya collisional suture; *6–10*, Early Mesozoic igneous complexes formed at the intraplate stage of tectogenesis: *6*, granite–leucogranites of the Kungurdzhara complex (T_2kg), *7*, lamprophyres and alkali basalts of the Chuya complex (T_2č), *8*, granite–leucogranites of the Kalguty complex (T_3–J_1kl), *9*, granite–leucogranites of the Chindagatui complex (J_1čn), *10*, granite porphyry, elvans, and ongonites of the East Kalguty complex (J_1vk); *11*, outlines of the Early Paleozoic Bukhtarma (in the west) and Kalguty (in the east) areals, mapped with regard to negative residual-gravity anomalies; *12–15*, hydrothermal and magmatogene rare-metal ore occurrences and deposits: *12*, essentially Mo, *13*, essentially W, *14*, Mo–W, *15*, Li–Ta; *16*, Early Mesozoic shears and reverse-normal faults; *17*, predominant kinematics of shears in geoblocks (lithons); *18*, state borders; *19*, plutons: 1, Chindagatui, 2, Orochagan, 3, Akalakha, 4, Tekekundei, 5, Kungurdzhara, 6, Kalguty.

Inset: Altai accretion–collision system, after Vladimirov et al. (2003, 2008), modified. *1*, Neoproterozoic–Early Paleozoic structure-lithologic complexes of the Siberian (SC) and Kazakhstan (KC) paleocontinents; *2*, Altai–Mongolian terrane (microcontinent); *3*, Rudny Altai and Zharma–Saur sea-margin–island-arc terranes; *4*, Kalba–Narym turbidite terrane; *5*, Chara oceanic terrane; *6*, Cenozoic deposits; *7*, undivided granitoids of Late Carboniferous to Early Jurassic age; *8*, undivided regional shears and faults: *a*, proved, *b*, predicted; *9*, Kalguty ore deposit.

centimeters to few meters in thickness (Fig. 3). The main phenocrysts in these rocks are K-feldspar, albite, quartz, and muscovite; single dikes contain biotite. Apatite and fluorite are subordinate but also abundant. The accessory minerals are pyrite, zircon, monazite, tantalite–columbite, xenotime, wolframite, montebrasite, herderite, and magnetite (Titov et al., 2001; Sokolova et al., 2011a,b).

Of special interest in this belt is the Tsentral'naya dike composed of ultrarare-metal varieties of ongonites and elvans (Annikova et al., 2006; Sokolova et al., 2011a,b).

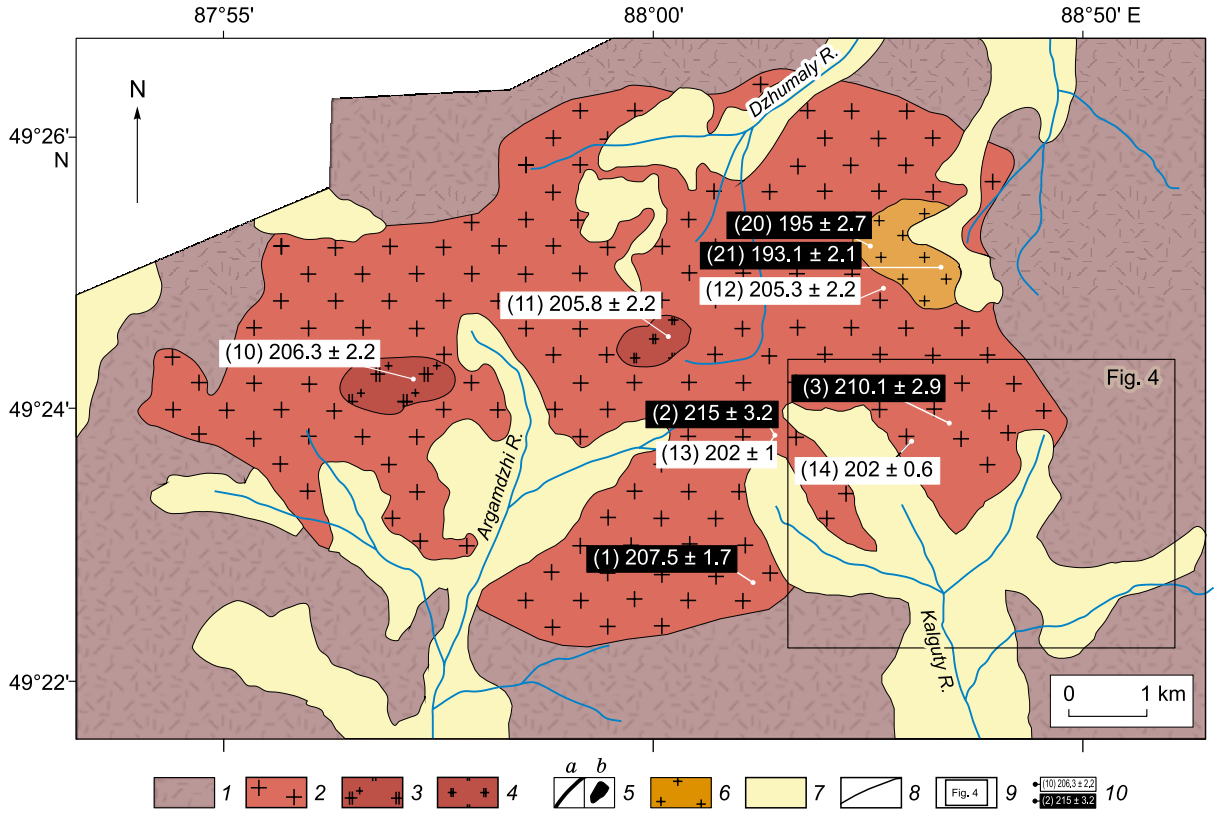

Fig. 2. Schematic geologic structure of the Kalguty rare-metal–granite batholith, after Annikova et al. (2006), modified. *1*, undivided Devonian volcanosedimentary deposit; *2*, porphyritic biotite granites of major intrusive phase; *3*, strongly porphyritic tourmaline-containing binary leucogranites (Argamdzha stock); *4*, porphyritic and(or) inequigranular binary leucogranites (Dzhumala stock); *5*, East Kalguty ongonite–elvan belt (*a*, dikes, *b*, plutons); *6*, coarse-grained muscovite leucogranites (Eastern stock); *7*, Quaternary deposits; *8*, geologic boundaries; *9*, outlined central part of the dike belt and the most productive prospecting site of the Kalguty deposit; *10*, sampling localities and results of isotope dating (black rectangles, U–Pb isotope dates, white rectangles, Ar–Ar isotope dates), parenthesized numbers follow Table 3.

Quartz veins of major Mo–W ore-productive stage are cut by elvans and ongonites; the opposite pattern is seldom observed. This led to a conclusion about the intra-ore type of dikes and their spatial and temporal association with a hydrothermal system (Annikova et al., 2007). The evolution of the Kalguty OMS was completed with the formation of thin ongonite and elvan dikes on the periphery of the ore field, which are associated with poor quartz–fluorite–barite–ferberite mineralization.

It should be emphasized that no one basic or lamprophyric dike was found within the Kalguty granitoid batholith or within the East Kalguty ongonite–elvan dike belt (Shokal'sky et al., 2000). This means that the Kalguty OMS that formed in the crust was a quasi-autonomous granite system. This intraplate geodynamic setting is unique for Altai and very seldom exists in other geologic structures of Central and Southeast Asia (Vladimirov et al., 2012a,b).

The Kalguty Mo–W deposit comprises two types of ore occurrences localized within the same ore field but differing in structural and geologic characteristics, chemical composition, and, obviously, isotopic (U/Pb, Re/Os, and $^{40}Ar/^{39}Ar$) ages.

The first type is Mo-rich mineralization in greisens and greisenized microgranites of the Molybdenum stock (Fig. 4). In the temporal sequence of ore-magmatic processes, the porphyry Mo mineralization is intimately associated with granitoids of major intrusive phase and precedes Mo–W quartz ore veins and greisens (Annikova et al., 2006; Potseluev et al., 2008; Gusev, 2011).

The second type of ore occurrence is the Kalguty deposit itself. It comprises a series of quartz ore veins and greisens on the southeastern margin of the granite batholith and at its exocontact (Fig. 4). Ore zone is ~2 km long and 0.5 km wide; the most productive site of the deposit spatially coincides with the axial zone of the East Kalguty dike belt (Tsentral'naya dike). Only 17 of the 600 known quartz ore veins and veinlets in the deposit have its balance ore reserves (they contain 70% of WO_3 and 75% of Mo reserves). These commercially important quartz ore veins are the thickest (on average, 1.5–2.0 m) and longest (on average, 300–350 m). Their main ore minerals are wolframite, molybdenite, chalcopyrite, beryl, and bismuthine, and the average contents of ore components are (wt.%): WO_3—2.81,

Mo—0.52, Be—1.14, Bi—0.11, and Cu—0.91. The most productive site of the Kalguty field is spatially associated with the Tsentral'naya dike (Fig. 4).

Chemical composition and thermobarogeochemical parameters of igneous rocks. The compositions of representative samples of igneous rocks from the Kalguty OMS are presented in Tables 1 and 2. Granites of major intrusive phase are medium-alumina rocks of normal alkalinity. On transition to leucogranites, the ASI and total alkalinity of the rocks increase, and most of the figurative points of the dike belt rocks correspond to subalkalic high-alumina compositions (Fig. 5*A*). On the quartz–albite–orthoclase–H_2O diagram (Fig. 5*B*), the normative-composition points of igneous rocks of the Kalguty OMS fall on the albite and elvan trends (Kovalenko and Kovalenko, 1976; Antipin et al., 1999, 2002; Sokolova et al., 2011a).

The $P_2O - \frac{(Li+Rb+Cs)F}{Sr+Ba}$ diagram shows a specific trend of ultrarare-metal ongonites and elvans of the East Kalguty dike belt (Fig. 5,*C*). On the transition from granites and leucogranites to elvans, ongonites, and ultrarare-metal ongonites, the contents of P_2O_5 drastically change. The rocks with the highest total content of trace alkaline elements and phosphorus compose the Tsentral'naya dike in the axial zone of the belt (Fig. 4). Within this dike, there are facies transitions between essentially sodic ($Na_2O > K_2O$) and essentially potassic ($K_2O > Na_2O$) ongonites. The potassic varieties have high contents of rare metals, and the sodic ones, ultrahigh contents. This indicates the heterogeneous composition of the dike belt as a whole and of the individual dikes as well as their genetic relationship because they are products of differentiation of the same parental magma in a deep-seated chamber (Sokolova et al., 2011b).

Study of melt and syngenetic fluid inclusions in porphyritic phenocrysts of quartz from rocks of the East Kalguty dike belt showed that the phenocrysts crystallized in a heterogeneous medium composed of silicate melt, crystals, and predominantly water fluid (Titov et al. 2001; Sokolova et al.,

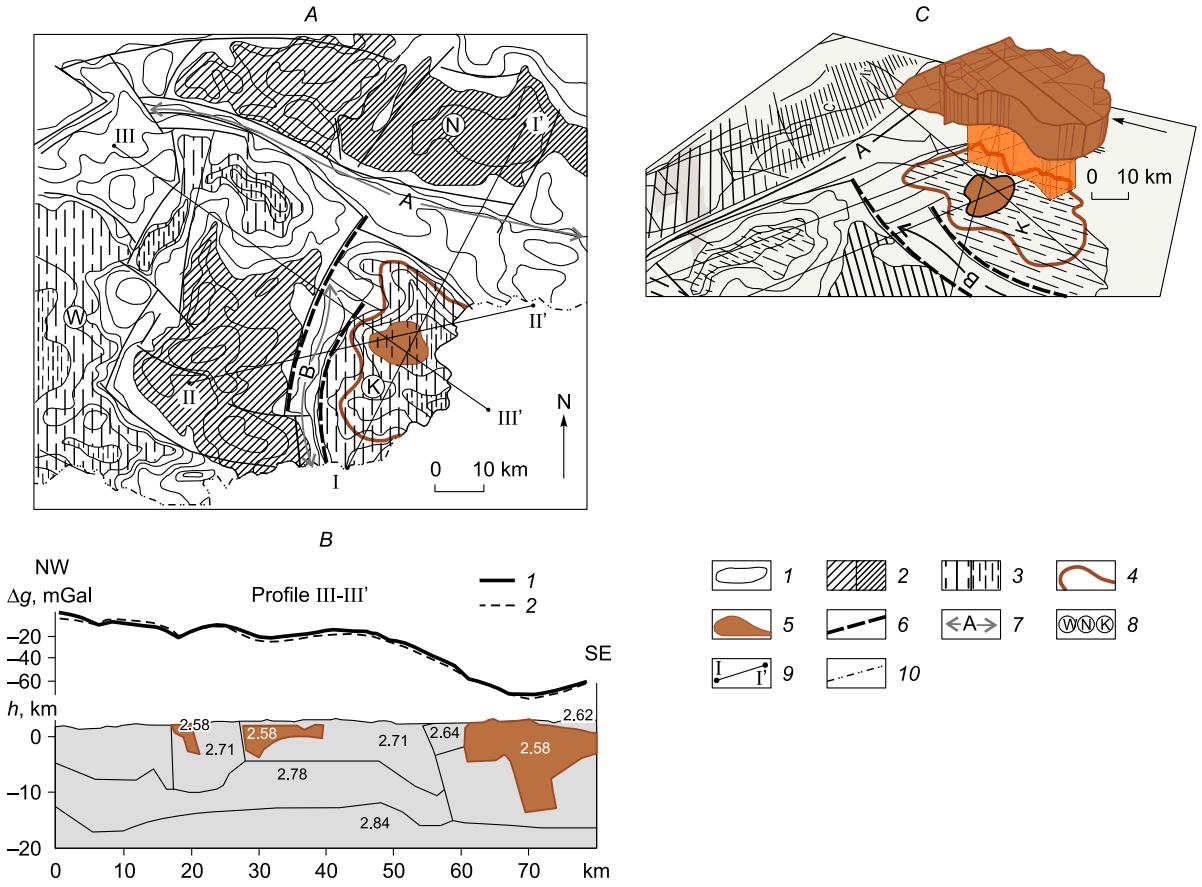

Fig. 3. Deep model of the Kalguty granite batholith, from geological and geophysical data (Annikova et al., 2004), supplemented. *A*, Scheme of zonation of local gravity anomalies in southern Gorny Altai, compiled by A.N. Vasilevsky (Annikova et al., 2004): *1*, isolines of gravity field intensity; *2*, *3*, gravity anomalies (hatching frequency marks the intensity of anomalies): relative maxima (*2*) and minima (*3*); *4*, outlined exposures of the Kalguty pluton; *5*, outlined buried pluton, from the modeling data; *6*, deep faults; *7*, gravity steps (A, B); *8*, crustal blocks (K, Kalguty; W, Western; N, Northern); *9*, calculated profiles; *10*, state border. B, Profile III–III′ (compiled by A.N. Vasilevsky) demonstrates the contrasting morphology of the pluton with an anomalous "stem" in its central part, reaching a depth of 10–12 km. The batholith flanks are 4–6 km in thickness. Numerals are the specific density of rocks (g/cm^3); Δg is the difference in the gravity field intensities: 1, observed Δg; 2, model Δg. *C*, Geometric 3D model of the Kalguty batholith with a granite "stem". Axonometric projections were compiled by I.A. Vladimirov, based on local gravity anomalies.

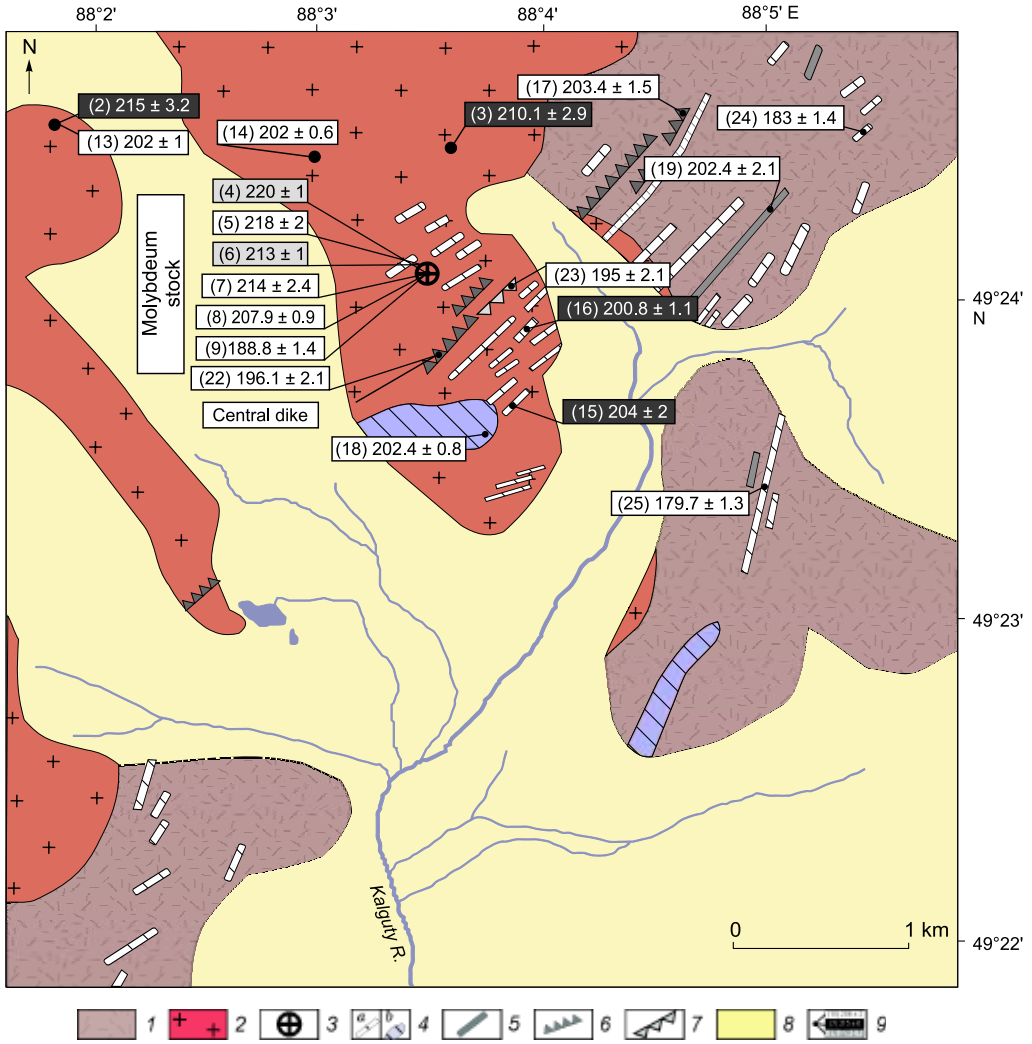

Fig. 4. Schematic map of the geologic structure of the East Kalguty dike belt, compiled by Dergachev (1988, 1989a), supplemented. *1*, undivided Devonian volcanosedimentary deposits; *2*, porphyritic biotite granites of major intrusive phase of the Kalguty pluton; *3*, Molybdenum stock; *4–7*, rocks of the East Kalguty dike belt: *4*, elvans (*a*, dikes; *b*, plutons), *5*, ongonites, *6*, ultrarare-metal ongonites, *7*, ultrarare-metal elvans; *8*, Quaternary deposits; *9*, sampling localities and results of isotope dating (black rectangles, U–Pb isotope dates; gray rectangles, Re–Os isotope dates; white rectangles, Ar–Ar isotope dates), parenthesized numbers follow Table 3.

2011a). The mineral formation environment was probably close in *P–T* conditions to the water-saturated solidus. The fluid pressure during the formation of quartz phenocrysts was estimated at 3.0 to 4.5–5.5 kbar, and the fluid temperature was 600–650 ºC. The temperature of crystallization of quartz phenocrysts in ultrarare-metal rocks of the dike belt was 20–30 ºC lower than that of phenocrysts in rocks with the lower total contents of rare alkaline metals (Sokolova et al., 2011a). Thus, the evolution of the residual chamber (magma chamber) was related to an active chemical interaction between granite melt and water fluid.

THERMOCHRONOLOGY

The history of a geochronological study of the Kalguty OMS. The first K–Ar dates for igneous rocks and orebodies of the Kalguty OMS were obtained under the guidance of V.N. Melenevskii at the Siberian Research Institute of Geology, Geophysics and Mineral Raw Materials, Novosibirsk, in the late 1970s–early 1980s (the samples were prepared by N.N. Amshinskii, V.B. Dergachev, etc.). The dating was made for monomineral fractions of muscovite (the most stable mineral in the K–Ar radiogenic system) sampled from granites of major phase, aplites, pegmatites, quartz–wolframite veins, and greisen rims and for bulk samples of vitreous varieties of ongonites and elvans. All estimated ages were within 197 ± 20 Ma (N = 19), which strongly contradicted the common views of the Permian age of the Kalguty OMS by analogy with the Kalba granites of Rudny Altai (Amshinskii, 1973). The first Rb–Sr isochron ages of the major-phase granites of the Kalguty OMS, the hosted minerals (K-feldspar, biotite, and apatite), elvans, and ongo-

Table 1. Chemical composition of representative samples of igneous rocks from the Kalguty OMS

Component	Stage I—granites of major phase and Molybdenum stock			Stage II—leucogranites of supplementary-intrusion phase				Stage III—ongonites and elvans of the East Kalguty dike belt				Stage IV—leucogranites of the Eastern stock and ultrarare-metal ongonites and elvans of the central part of the dike belt				Stage V—elvans on the dike belt periphery	
	215 ± 1 Ma			206 ± 1 Ma				202±1 Ma				195±1 Ma				181±1 Ma	
	Porphyritic biotite granites			Leucogranites				Ongonites		Elvans		Tsentral'naya dike		Muscovite leucogranites		Elvans	
				Argamdzha stock		Dzhumala stock						Ultrarare-metal ongonite	Ultrarare-metal elvan				
	1-271	1-277	P-678*	L-448	L-449/1	KL-341/1	L-741/1	KL-15	1-262/3	1-278	683-11*	KL-211	KL-209	L-503	10137*	KL-121	KYu-8
SiO_2, wt.%	70.91	70.33	73.80	73.93	74.07	72.46	74.32	72.95	72.18	72.78	74.70	71.73	73.69	76.21	76.10	73.25	72.54
TiO_2	0.41	0.49	0.40	0.13	0.17	0.15	0.05	0.05	0.06	0.08	0.07	0.04	0.08	0.13	0.13	0.08	0.06
Al_2O_3	14.27	14.36	13.80	14.64	14.04	14.11	13.94	14.40	14.82	14.87	14.40	15.65	14.90	13.21	13.40	14.85	14.34
Fe_2O_{3tot}	2.42	2.86	2.29	1.27	1.29	1.97	1.12	1.48	0.88	0.93	0.75	1.05	0.92	1.43	0.79	1.16	1.02
MnO	0.08	0.09	0.07	0.09	0.09	0.06	0.06	0.11	0.09	0.11	0.03	0.09	0.08	0.06	0.05	0.15	0.08
MgO	0.67	0.79	0.64	0.23	0.31	0.28	0.40	0.12	0.10	0.14	0.10	0.13	0.10	0.05	0.24	0.24	0.17
CaO	1.52	1.62	1.42	0.77	0.79	0.69	0.84	0.48	0.62	0.61	0.48	0.82	0.60	0.63	0.86	0.58	0.51
Na_2O	2.98	3.62	2.72	3.78	3.68	3.33	3.79	4.65	6.02	3.60	3.82	4.29	3.80	3.41	3.70	4.09	3.64
K_2O	4.76	5.10	4.43	4.20	4.48	4.78	3.90	4.26	3.92	4.87	4.72	3.35	4.40	4.11	4.15	4.39	5.45
P_2O_5	0.19	0.21	0.19	0.19	0.20	0.21	0.33	0.38	0.48	0.28	0.31	0.66	0.32	0.08	0.08	0.34	0.35
LOI	0.64	0.72	0.50	0.71	0.86	0.92	0.96	0.55	0.92	0.84	0.74	1.89	0.83	0.74	0.70	0.60	1.29
Total	98.85	100.19	100.30	99.94	99.98	98.96	99.81	99.42	100.09	99.11	100.10	99.71	99.72	100.06	100.20	99.74	99.45

Note. Contents of oxides were determined by XRF at the Analytical Center for Multielemental and Isotope Research of the Institute of the V.S. Sobolev Institute of Geology and Mineralogy, Novosibirsk.
* Data by Gusev (2011).

nites were obtained by V.A. Ponomarchuk (oral report) in the Geochronological Laboratory of the Institute of Geology and Geophysics, Novosibirsk, in 1980. It agreed with the above ages: 204 ± 2 Ma; $(^{87}Sr/^{86}Sr)_0 = 0.70688 \pm 14$; and MSWD = 0.22 (the samples were prepared by A.A. Obolensky and G.E. Dashkevich). Note that the granites were sampled within the Kalguty ore deposit, and the obtained age, most likely, corresponds to the rebuilding of the Rb–Sr radiogenic system during the greisenization of igneous wall-rocks. Like the K–Ar ages, this estimate was not correctly explained and thus was not published.

Today, there are fundamentally new analytical instruments and techniques for a geochronological study of the Kalguty OMS (U/Pb isotope dating (SHRIMP-II) of zircons and $^{40}Ar/^{39}Ar$ isotope dating of minerals by stepwise heating) (Baksi et al., 1996; Williams, 1998; Black and Kamo, 2003; Travin et al., 2009).

U/Pb isotope dating. Geochronological studies were performed independently by the geologists of the Institute of Geology and Mineralogy, Novosibirsk (Annikova et al., 2006), and of the Russian Geological Research Institute (VSEGEI), St. Petersburg (Gusev, 2011). In the first case, the sample 1-271 taken beyond the Kalguty ore field was studied (Figs. 2 and 4). In the second case, systematic zirconometry of all types of igneous rocks of the Kalguty OMS was performed, with the main attention paid to the Kalguty ore field (Gusev, 2011). The age of the Eastern stock (193–195 Ma) was the most unexpected result, but its coincidence with the age of the ultrarare-metal ongonite–elvans of the Tsentral'naya dike and the geologic structure of the ore field leave no doubt about the age reliability. This is confirmed by geological observations showing that the Eastern stock is proximal to the Kalguty ore field and the ongonite–elvan dike belt (Figs. 2 and 4). Abundant intragranitic schlieric and vein pegmatites with tourmaline, muscovite, fluorite, and beryl are confined to this stock, with the number of pegmatites decreasing with distance from the ore field. The younger age of the intrusion of binary leucogranites in the Eastern stock, their ore-generating capacity, and the possible regeneration of early porphyry Mo mineralization might be among the causes of the superposition of greisen mineralization on the elvan and ongonite dikes (Gusev, 2011).

$^{40}Ar/^{39}Ar$ isotope dating. One of the main tasks was to study as more as possible igneous rocks and orebodies both within the Kalguty ore field and beyond it, including the hardly accessible Argamdzha and Dzhumala intrusive leucogranite stocks (Fig. 2). Samples for $^{40}Ar/^{39}Ar$ dating were taken from the least greizenized igneous rocks and(or) rocks least subject to secondary alterations (Fig. 6*A*). Special attention was focused on muscovites and muscovite–phengites with high contents of Li, Rb, and F (Fig. 6*B*). These minerals in intrusive leucogranite stocks and elvan–ongo-

Table 2. Contents of F, B, and trace and rare-earth elements in representative samples of igneous rocks from the Kalguty OMS

Element	Stage I—granites of major phase and Molybdenum stock			Stage II—leucogranites of supplementary-intrusion phase				Stage III—ongonites and elvans of the East Kalguty dike belt				Stage IV—leucogranites of the Eastern stock and ultrarare-metal ongonites and elvans of the central part of the dike belt				Stage V—elvans on the dike belt periphery	
	215 ± 1 Ma			206 ± 1 Ma				202 ± 1 Ma				195 ± 1 Ma				181 ± 1 Ma	
	Porphyritic biotite granites			Leucogranites				Ongonites		Elvans		Tsentral'naya dike		Muscovite leucogranites		Elvans	
				Argamdzha stock		Dzhumala stock						Ultrarare-metal ongonite	Ultrarare-metal elvan				
	1-271	1-277	P-678*	L-448	L-449/1	KL-341/1	L-741/1	KL-15	1-262/3	1-278	683-11*	KL-211	KL-209	L-503	10137*	KL-121	KYu-8
F	0.15	0.14	–	0.07	0.07	–	0.12	0.24	0.26	0.26	–	0.57	0.23	0.11	–	0.44	0.43
B	–	–	–	–	–	–	35	35	–	–	–	0.57	40	–	–	81	110
Li	–	101	348	155	167	–	–	150	275	332	122	1645	540	130	70.1	395	220
Rb	360	223	281	220	267	384	400	648	666	623	584	1307	578	441	413	650	680
Cs	29.4	34.4	28.1	47	81	25	21	100	185	76.4	120	512	160	33	17.1	139	51
Be	–	2.55	–	14	9	–	6.4		42.1	23		97	52	8	–	58	–
Nb	35.8	24.7	31.2	46	32	28	13	67	64.6	43	58	77	47	100	51.6	52	42
Ta	3.00	3.28	2.86	–	–	5.1	–	40	40.9	11.4	12	71	16		9.72	22	15.2
Sr	123	103	127	110	140	60	98	66	31.3	20	24	140	33	63	29.9	31	56
Ba	320	347	650	360	540	131	180	75	38.1	54.9	46	30	81	200	42.7	82	114
Mo	–	–	3.8	2.5	3.3	–	12	–	–	–	–	0.58	0.7	22	1.02	0.6	–
Sn	–	–	–	5.1	–	–	–	–	–	–	–	1.3	2.5	–	–	1.6	–
W	–	21.9	8.71	7.5	13	–	95	–	–	–	–	27	–	–	16.8	16	–
Y	36.4	24.9	34.4	26	40	17.8	1	11.0	4.7	9.2	8.85	10.6	18.2	19	25.1	9.8	7.3
Zr	208	52.6	224	180	140	96	24	37	24.9	28.9	36.3	24	41	170	49.2	40	25
Hf	4,70	2.03	6.03	–	–	2.9	–	1.75	1.81	1.1	1.38	1.97	1.91	–	2.03	1.94	1.62
Th	23	22	23	–	–	15.9	–	4.3	3.69	4.8	3.33	2.0	6.2	–	11.9	7.2	4.4
U	11.7	3.72	7.1	–	–	8.8	–	27	13.6	2.3	4.55	25	39	–	25	19.8	13.4
La	44.1	25.8	41.1	–	–	18.9	–	5.3	4.0	8.9	4.85	2.3	7.2	–	25	9.0	6.4
Ce	74.6	55.1	86.3	–	–	41	–	11.2	8.91	17.2	11.0	5.2	15.6	–	55	19.7	12.9
Pr	–	7.67	10.2	–	–	5.0	–	1.56	0.99	2.03	1.21	0.69	2	–	6.72	2.2	1.68
Nd	35.2	29.3	36.3	–	–	17.3	–	6.0	3.8	6.82	4.75	3.1	7.9	–	25	8.0	5.7
Sm	8	6.06	7.68	–	–	3.6	–	1.56	0.7	1.32	1.17	1.03	2.1	–	5.81	1.82	1.41
Eu	1	1	1.08	–	–	0.45	–	0.21	0.1	0.18	0.17	0.17	0.26	–	0.5	0.22	0.14
Gd	7.5	5.47	6.8	–	–	3.2	–	1.57	0.71	1.27	1.18	1.41	2.3	–	4.98	1.58	1.32
Tb	1.27	0.92	0.99	–	–	0.51	–	0.25	0.14	0.25	0.24	0.26	0.43	–	0.73	0.27	0.25
Dy	–	4.95	5.8	–	–	2.9	–	1.65	0.76	1.48	1.33	1.58	2.9	–	4.2	1.66	1.70
Ho	–	1.07	1.16	–	–	0.57	–	0.32	0.16	0.31	0.28	0.29	0.58	–	0.84	0.29	0.31
Er	–	2.9	3.27	–	–	1.68	–	0.95	0.42	0.94	0.8	0.85	1.88	–	2.54	0.87	0.94
Tm	–	0.46	0.48	–	–	0.28	–	0.15	0.07	0.17	0.14	0.14	0.31	–	0.39	0.15	0.18
Yb	3.78	2.82	3.29	–	–	1.82	–	1.01	0.49	1.05	1.04	0.92	2.2	–	3.37	1.12	1.13
Lu	0.55	0.39	0.48	–	–	0.28	–	0.14	0.08	0.15	0.18	0.14	0.34	–	0.5	0.15	0.18

Note. Contents of F are in wt.%, and contents of the other elements are in ppm; dash, no data. Contents of trace and rare-earth elements were determined by ICP-MS at the Analytical Center for Multielemental and Isotope Research of the Institute of the V.S. Sobolev Institute of Geology and Mineralogy, Novosibirsk, and contents of F, B, Li, Rb, Cs, Be, W, Cu, Zn, Ge, Mo, Ag, Sn, Tl, and Pb, by quantitative AES at the Analytical Center of the Institute of Geochemistry, Irkutsk.

* Data by Gusev (2011).

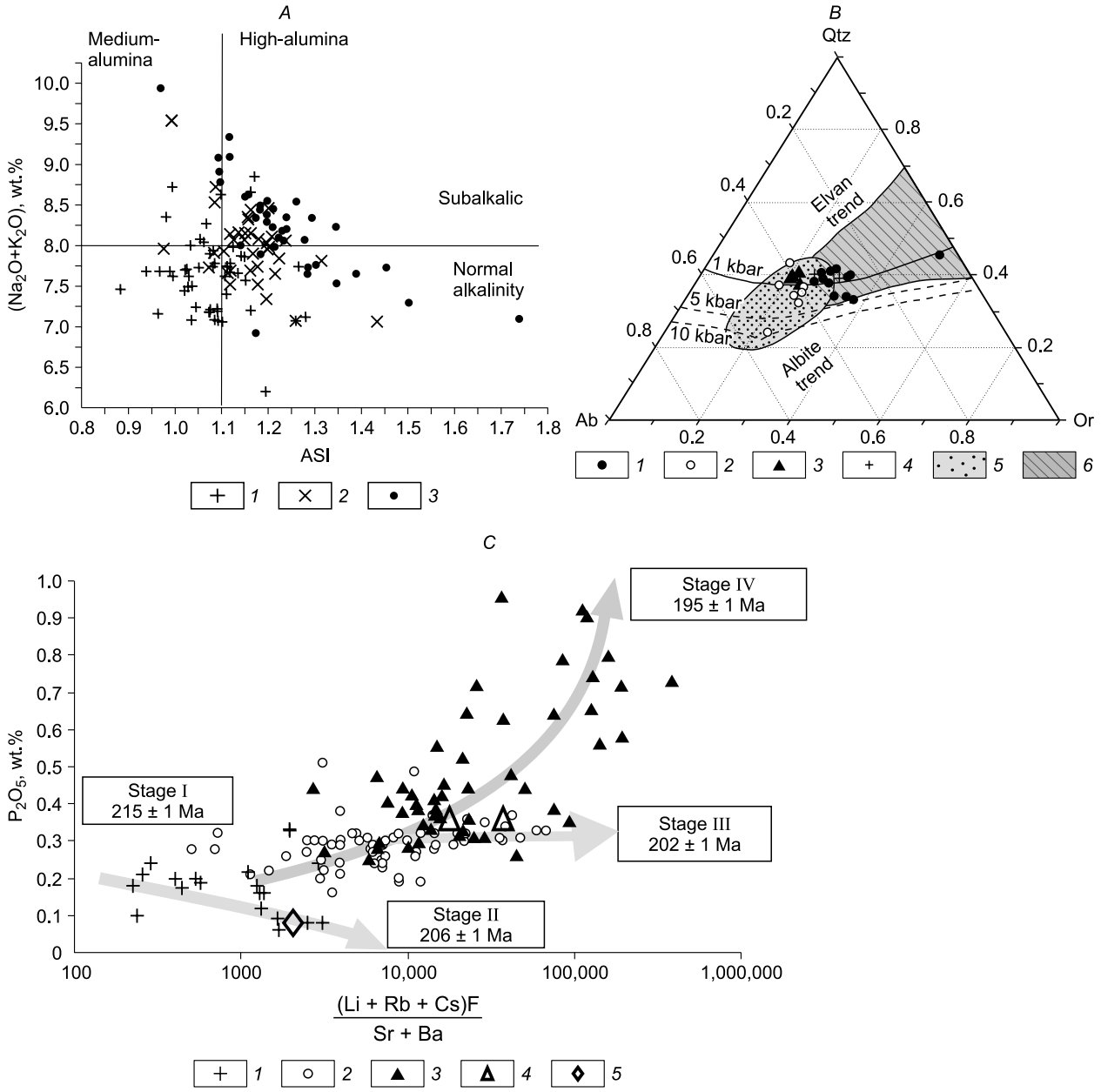

Fig. 5. Geichemical composition of granites, ongonites, and elvans of the Kalguty OMS. *A*, ($Na_2O + K_2O$)–ASI composition diagram for intrusive rocks of the Kalguty OMS. (ASI) = A/CNK, Aluminum saturation index (Zen, 1986): *1*, granites; *2*, leucogranites; *3*, ongonites and elvans. *B*, Normative quartz–albite–orthoclase–H_2O normative composition diagram for intrusive rocks of the Kalguty OMS: *1*, elvans; *2*, ongonites; *3*, ultrarare-metal ongonites; *4*, granites of major intrusive phase; *5*, composition field of Mongolian and Cisbaikalian ongonites (Kovalenko and Kovalenko, 1976; Antipin et al., 1999); *6*, composition field of the Cornwall elvans (Antipin et al., 2002). *C*, $P_2O_5 - \frac{(Li+Rb+Cs)F}{Sr+Ba}$ diagram for intrusive rocks of the Kalguty OMS: *1*, porphyritic biotite granites of major phase and leucogranites of the Argamdzha and Dzhumala stocks; *2*, ongonites and elvans; *3*, ultrarare-metal ongonites and elvans; *4*, elvans of the dike belt periphery; *5*, leucogranites of the Eastern stock. Arrows show the composition evolution trends of rocks of the Kalguty OMS. For other designations, see the text.

nite dikes were proved to be of magmatic origin (Titov et al., 2001; Annikova et al., 2006; Sokolova et al., 2011a). Orebodies were studied using syngenetic micas of hydrothermal genesis (greisens and quartz ore veins).

Mineral fractions were separated by the standard methods of magnetic and density separation. $^{40}Ar/^{39}Ar$ isotope studies by the stepwise-heating method were performed at the Analytical Center for Multielemental and Isotope Re-

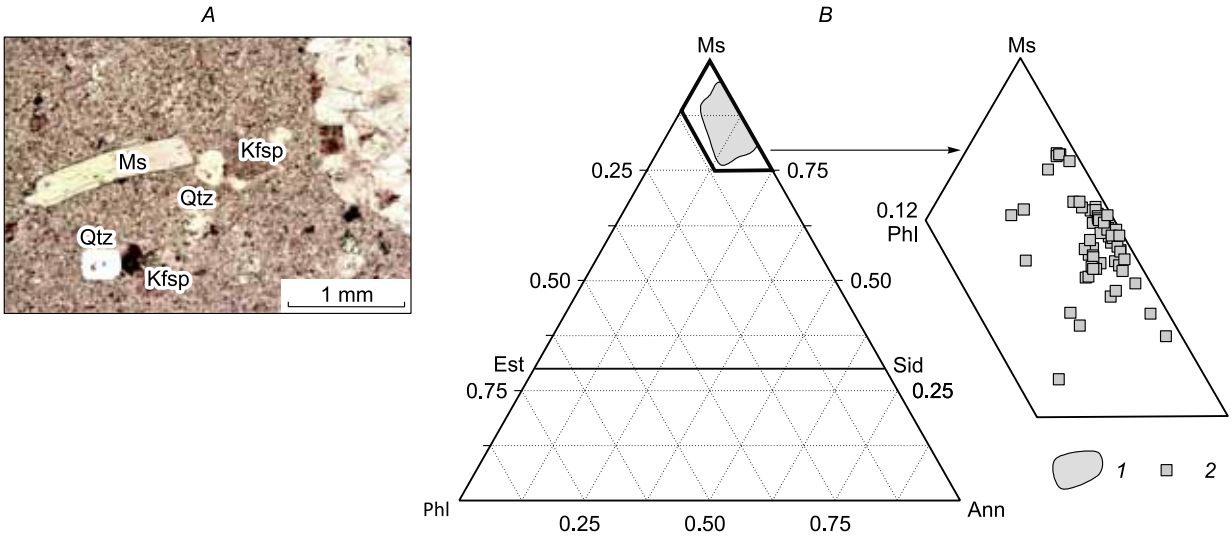

Fig. 6. Morphology of phenocrysts (*A*) and composition (*B*) of magmatic muscovites from rocks of the East Kalguty dike belt, which were used for $^{40}Ar/^{39}Ar$ dating. Kfsp, K-feldspar; Qtz, quartz; Ms, muscovite; Ann, annite; Est, eastonite; Sid, siderophyllite; Phl, phlogopite. Mineral abbreviations are given after Kretz (1983). *1*, composition field of muscovites; *2*, figurative composition points of muscovites.

search of the V.S. Sobolev Institute of Geology and Mineralogy, Novosibirsk. The samples for study, together with muscovite MSA-11 (age of 311.0 ± 1.5 Ma) used as a monitor and calibrated against the international standard LP-6 biotite and Bern-4m muscovite samples (Baksi et al., 1996), were wrapped in aluminum foil and placed in a quartz ampoule, which was evacuated and sealed. Then the samples were irradiated in the cadmium channel of a WWR-K reactor at the Institute of Physics and Technology of Tomsk Polytechnic University. The neutron flux gradient did not exceed 0.5% of the sample size. Stepwise-heating experiments were carried out in a quartz reactor with an external-heating furnace. The blank experiment carried out at 1200 ºC for 10 min revealed no more than 5×10^{-10} ncm^3 ^{40}Ar. Argon was purified with ZrAl–SAES getters. The isotopic composition of argon was measured on a Noble gas 5400 Micromass (England) mass spectrometer. The measurement errors were within ±1σ. Correction for interfering argon isotopes formed during Ca, Cl, and K irradiation was made using the following coefficients: $(^{39}Ar/^{37}Ar)_{Ca} = 0.000891 \pm 0.000003$, $(^{36}Ar/^{37}Ar)_{Ca} = 0.000446 \pm 0.000004$, and $(^{40}Ar/^{39}Ar)_K = 0.089 \pm 0.001$. Before measurements, the samples were outgassed at 350 ºC. The isotope discrimination of the mass spectrometer was controlled by a regular measurement of $^{40}Ar/^{36}Ar$ in portions of cleaned atmospheric argon. The average $^{40}Ar/^{36}Ar$ value over the measurement period was 299 ± 1. The age and Ca/K spectra were interpreted using the age plateau method (Fleck et al., 1977), which permits calculation of the weighted average age for several sequential (at least three) temperature steps with consistent age values close to the Ca/K ratios. The portion of released ^{39}Ar corresponding to the plateau must be no smaller than 50%.

All the obtained age spectra (Figs. 7 and 8) have distinct plateaus. The weighted average plateau ages are taken as the time of the closure of the K/Ar radiogenic system in the corresponding geochronometer minerals.

The estimated ages are as follows: muscovites from the leucogranites of the Dzhumala and Argamdzha stocks, 206 ± 2 and 207 ± 2 Ma, respectively; biotites from the granites of major phase and associated pegmatites, 202 ± 1 Ma and 202 ± 1 Ma, respectively (Figs. 2 and 7*A–E*). With regard to the analytical error, we could assume that these minerals formed during the same magmatic event, but the obtained zirconometry data point to their different geologic nature (see below).

Three statistically isolated age groups have been established for the East Kalguty dike belt. The most "ancient" ages, falling in the narrow interval 202–203 Ma, were obtained for ongonites exposed on the northeastern flank, within one of the exploration sites of the Kalguty deposit (Figs. 4 and 8*A–C*). Two age estimates for the Tsentral'naya ultrarare-metal dike in the axial part of the belt are close: elvans—195 ± 2 Ma, ongonites—196 ± 2 Ma (Figs. 4 and 8*D*, *E*). The youngest ages in the East Kalguty dike belt (180 ± 1 Ma and 184 ± 1 Ma) were obtained for elvans of the southeastern and eastern flanks of the belt (Figs. 4 and 8*F*, *G*). Note that all sampled dikes are not subject to greisenization and other postmagmatic secondary alterations, which permits us to regard their ages as the time of crystallization of ongonite–elvan melts.

A geochronological study of orebodies was carried out in the Molybdenum stock, where almost all stages of the ore-hydrothermal processes running at the Kalguty deposit have been established. The most "ancient" ages were obtained by Re–Os molybdenite dating: 220 ± 1 and 213 ± 1 Ma (Berzina et al., 2003). The $^{40}Ar/^{39}Ar$ isotope dating of muscovites from greisens and quartz Mo–W ore veins yielded a wider range of values, 214–208 Ma (Figs. 4 and 7*F*, *G*). The

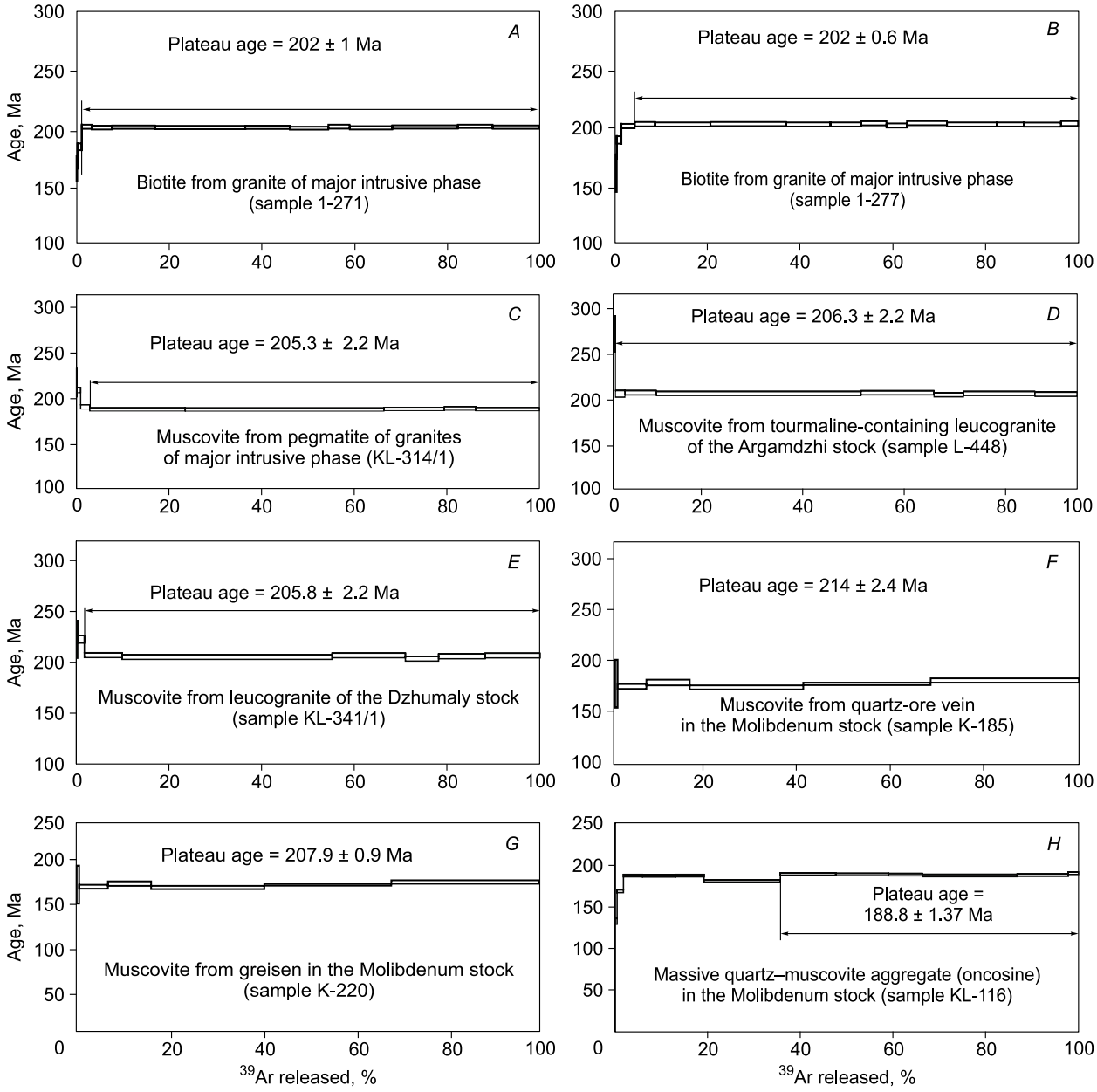

Fig. 7. $^{40}Ar/^{39}Ar$ age spectra of muscovites and biotites from granite–leucogranites of the Kalguty granitoid batholith and orebodies of the Molybdenum stock. *A–H*, For explanation, see the text.

plateau age of massive molybdenite–quartz–muscovite aggregates (oncosine) is 189 ± 1 Ma (Figs. 4 and Fig. 7*H*). The last date confirms the conclusion by Guseva (2011) about the regeneration of porphyry Mo mineralization at the Kalguty deposit.

Stages and duration of the formation of the Kalguty OMS. The Kalguty OMS is characterized by multistage magmatic and ore-forming processes with a considerable time gap. Under these conditions, the isotope dates for minerals and systems with different stabilities can vary widely depending on the thermal history and the intensity of superposed effects. The greater number of dates is expected for more intense events (superposed heating, drastic drop in temperature, etc.) because of the higher probability of the complete rejuvenation and closure of the system. Thus, the coincidence of dates for the isotope systems of different minerals suggests their likely correspondence to the age of a real geologic event. This is a basis for the pair criteria, namely, the coincidence of the K/Ar ($^{40}Ar/^{39}Ar$) age of two (or more) minerals with the good preservation of radiogenic argon (Shanin, 1979; Morozova and Rublev, 1987). The proposed principles were used to interpret the results of integrated dating of a wide range of isotope systems and minerals. In our case, it is U/Pb (zircon), $^{40}Ar/^{39}Ar$ (biotite, muscovite), and Re/Os (molybdenite) dating. The general geochronological data are given in Table 3. The thermo-

Table 3. Geochronological summary of literature and the authors' U/Pb, Re/Os, and Ar/Ar isotope dates for rocks and orebodies of the Kalguty OMS

No.	Rock	Sample	Method, mineral	Age, Ma	Reference
Stage I—granites of major intrusive phase and the Molybdenum stock with Mo-rich mineralization					
1	Porphyritic biotite granite at a distance from the deposit ore field	P-068	U–Pb, SHRIMP II, zircon	207.5 ± 1.7	(Gusev, 2011)
2	Porphyritic biotite granite on the periphery of the deposit ore field	1-271	U–Pb, SHRIMP II, zircon	215.0 ± 3.2	(Annikova et al., 2006)
3	Porphyritic biotite granite in the deposit ore field	P-678	U–Pb, SHRIMP II, zircon	210.1 ± 2.9	(Gusev, 2011)
4	Quartz–molybdenite–chalcopyrite vein in the Molybdenum stock	R-220	Re–Os, molybdenite	220.0 ± 1	(Berzina et al., 2003)
5	Quartz–molybdenite–chalcopyrite vein in the Molybdenum stock	—	Ar–Ar, muscovite	218.0 ± 2	(Seltmann et al., 2007)
6	Quartz–molybdenite–wolframite vein in the Molybdenum stock	K-209	Re–Os, molybdenite	213.0 ± 1	(Berzina et al., 2003)
7	Quartz–molybdenite–wolframite vein in the Molybdenum stock	K-185	Ar–Ar, muscovite	214.0 ± 2.4	(Seltmann et al., 2007)
8	Quartz–muscovite greisen with sulfides in the Molybdenum stock	K-220	Ar–Ar, muscovite	207.9 ± 0.9	
9	Massive quartz–muscovite aggregate (oncosine) in the Molybdenum stock	KL-116	Ar–Ar, rock	188.8 ± 1.4	(Annikova et al., 2014)
Stage II—leucogranites of supplementary intrusions (Argamdzhi and Dzhumaly stocks) and intragranitic pegmatites					
10	Tourmaline-containing binary leucogranite of the Argamdzha stock	L-448	Ar–Ar, muscovite	206.3 ± 2.2	(Annikova et al., 2014)
11	Binary leucogranite of the Dzhumala stock	KL-341/1	Ar–Ar, muscovite	205.8 ± 2.2	(Annikova et al., 2014)
12	Pegmatite in major-phase granites	KL-314/1	Ar–Ar, muscovite	205.3 ± 2.2	(Annikova et al., 2014)
Biotite threshold of the K–Ar system in major-phase granites					
13	Porphyritic biotite granite of major phase on the periphery of the deposit ore field	1-271	Ar–Ar, biotite	202.0 ± 1	(Annikova et al., 2006)
14	Porphyritic biotite granite of major phase in the deposit ore field	1-277	Ar–Ar, biotite	202.0 ± 0.6	(Annikova et al., 2006)
Stage III—ongonites and elvans of the East Kalguty dike belt					
15	Elvan (deposit ore field)	683-11	U–Pb, SHRIMP II, zircon	204.0 ± 2	(Gusev, 2011)
16	Ultrapotassic rhyolite porphyry (deposit ore field)	678-2	U–Pb, SHRIMP II, zircon	200.8 ± 1.1	(Gusev, 2011)
17	Ongonite (northeastern part of the belt within one of the deposit exploration sites)	1-262/3	Ar–Ar, muscovite	203.4 ± 1.5	(Annikova et al., 2006)
18	Elvan (massif in the central part of the dike belt)	1-278	Ar–Ar, muscovite	202.4 ± 0.8	(Annikova et al., 2006)
19	Ongonite (northeastern part of the belt within one of the deposit exploration sites)	KL-15	Ar–Ar, muscovite	202.4 ± 2.1	(Annikova et al., 2014)
Stage IV—leucogranites of the Eastern stock, ultrarare-metal ongonites and elvans of the central part of the dike belt and W-rich mineralization					
20	Muscovite leucogranite of the Eastern stock	10136	U–Pb, SHRIMP II, zircons	195.0 ± 2.7	(Gusev, 2011)
21	Muscovite leucogranite of the Eastern stock	10137	U–Pb, SHRIMP II, zircons	193.1 ± 2.1	(Gusev, 2011)
22	Ultrarare-metal ongonite from a long dike in the central part of the belt	KL-211	Ar–Ar, muscovite	196.1 ± 2.1	(Annikova et al., 2014)
23	Ultrarare-metal elvan from the same dike	KL-209	Ar–Ar, muscovite	195.0 ± 2.1	(Annikova et al., 2014)
Stage V—elvans on the periphery of the dike belt					
24	Elvan (northeastern flank of the belt)	KL-121	Ar–Ar, muscovite	184.3 ± 1.4	(Annikova et al., 2014)
25	Large-phenocryst elvan (southeastern flank of the belt)	KYu-8	Ar–Ar, muscovite	179.7 ± 1.3	(Annikova et al., 2014)

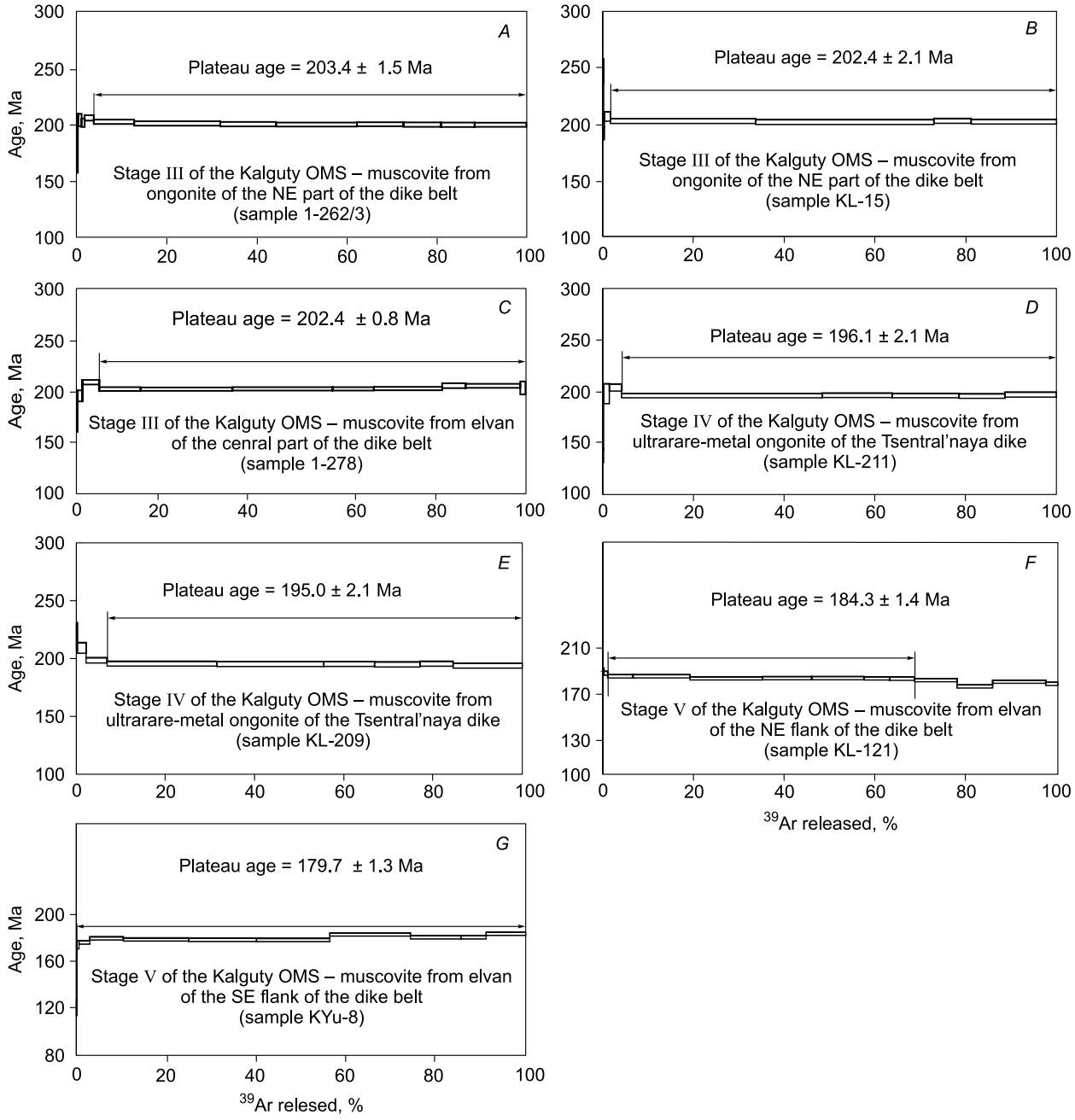

Fig. 8. $^{40}Ar/^{39}Ar$ age spectra of muscovites from ongonites and elvans of the East Kalguty dike belt. *A–G*, For explanation, see the text.

chronogram of real geologic events is presented in the coordinates temperature–age of the closure of radiogenic systems in Fig. 9. This diagram permits one to estimate the statistical peaks of the ages and, as a result, pass to a geological scenario. We have reconstructed the most likely history of the thermal cooling of the Kalguty OMS (Fig. 10), based on a joint analysis of geological observations, thermochronology, and the physicochemical conditions of differentiation and cooling of granite melts.

Stage I ((215 ± 1 Ma). The age of granites of major intrusive phase of the Kalguty granitoid batholith determined by U/Pb zircon (SHRIMP-II) dating (three dates) is within 215–207 Ma (Gusev, 2011). At the same time, it must not be younger than the ore veins cutting the granites, whose Re/Os age is 220 ± 1 and 213 ± 1 Ma and age determined by $^{40}Ar/^{39}Ar$ muscovite dating is 218 ± 2 and 214 ± 2 Ma (Table 3). Thus, the age of the major-phase granites is apparently 215 ± 1 Ma (the average over the above isotope dates).

$^{40}Ar/^{39}Ar$ biotite dating of the major-phase granites yielded a much younger age, 202 ± 2 Ma, which cannot be explained by the rejuvenation of the K/Ar radiogenic system of the biotites during the intrusion of numerous dikes of the East Kalguty belt, because the granites were sampled both within and beyond the ore field (Figs. 2 and 4) and are free

of traces of postmagmatic recrystallization and greisenization (Annikova et al., 2006). In Fig. 10, these dates are presented as the "biotite threshold" of the closure of the K/Ar isotope system during the denudation of the roof of the Kalguty batholith and, as a result, its cooling. This geologic event apparently reflects the extension of the South Altai continental lithosphere, which was accompanied by the tectonic rise of the already crystallized granitoid batholith, on the one hand, and by subsynchronous intrusions (Arghamdzha and Dzhumala stocks) and the formation of the most "ancient" microgranite porphyry and ongonite–elvan dikes of the East Kalguty dike belt, on the one hand.

Stage II (206 ± 1 Ma). $^{40}Ar/^{39}Ar$ muscovite dating of leucogranites from the Argamdzha and Dzhumala stocks located far from the ore field and of the intragranitic pegmatites yielded consistent ages (206 ± 2, 206 ± 2, and 205 ± 2 Ma, respectively, Table 3, Fig. 10), which increases the degree of their reliability. These results can be interpreted either as the age of magmatic events or as the age of the closure of the K/Ar isotope system of muscovites during the tectonic rise of the granite batholith to the upper crust. We tentatively accepted the first variant, but the final solution of this issue requires additional combined U/Pb and $^{40}Ar/^{39}Ar$ dating of igneous bodies.

Stage III (202 ± 1 Ma). U/Pb zircon dating of microgranite porphyry and ongonite–elvans composing most of the East Kalguty belt and showing an autonomous geochemical trend on indicator diagrams (Fig. 5) yielded two ages (204 ± 2 and 201 ± 1 Ma, respectively), and $^{40}Ar/^{39}Ar$ dating of magmatic muscovites yielded three ages (Table 3, Fig. 10). These dates agree within the analytical errors and unambiguously mark the beginning of formation of the East Kalguty dike belt.

Stage IV (195 ± 1 Ma). Analysis of the obtained geological and geochronological data (Annikova et al., 2006; Gusev, 2011) (Table 3, Fig. 10) shows that the formation of the Kalguty Mo–W ore deposit was almost synchronous with the intrusion of the Eastern leucogranite stock and the Tsentral'naya ultrarare-metal ongonite–elvan dike and the

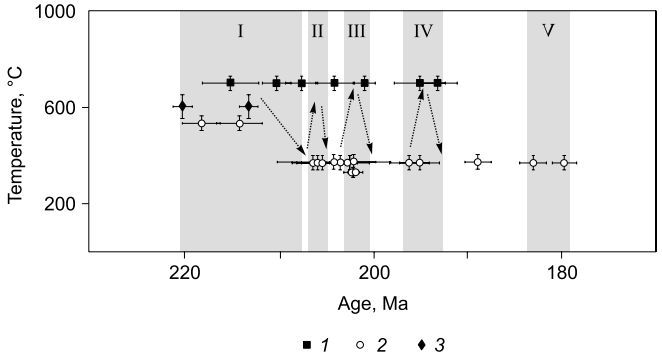

Fig. 9. Multisystem and multimineral thermochronogram depicting the temperature and age of the closure of radiogenic systems in the Kalguty OMS minerals. *1*, U–Pb isotope dating of zircons (SHRIMP-II); *2*, Ar–Ar isotope dating of micas; *3*, Re–Os isotope dating of molybdenum.

Table 4. Physical properties of minerals taken for numerical modeling of the thermal history of the Kalguty OMS

Mineral*	Thermal conductivity, W/(m·K)	Heat capacity, J/(kg·K)	Density, g/cm^3
Quartz	7.99	750.0	2.65
Albite	2.31	711.0	2.61
Orthoclase	2.31	628.0	2.55
Augite	3.82	748.8	3.40

* The physical parameters are borrowed from Dortman (1984).

associated bodies and satellites (Fig. 4). The U/Pb age of two samples of Eastern stock granites is 195 ± 3 and 193 ± 2 Ma (Table 3). $^{40}Ar/^{39}Ar$ muscovite dating of ongonites and elvans of the Tsentral'naya dike yielded ages equal within the analytical error, 196 ± 2 and 195 ± 2 Ma. Note that the ongonite and elvan facies of the Tsentral'naya dike are characterized by gradual transitions, which is due to crystallization differentiation in the presence of magmatic fluid in magma chamber. Earlier, this process was established in the Ary-Bulak ongonite–elvan stock in Transbaikalia (Antipin et al., 2009).

Stage V (181 ± 1 Ma). The Kalguty ore field has a zonal structure. Most of ongonite–elvan dikes are spatially conjugate with the Kalguty Mo–W deposit (ore column), whereas its periphery has occasional elvan dikes spatially associated with poor quartz–fluorite–barite–ferberite veins (Fig. 4). $^{40}Ar/^{39}Ar$ dating of magmatic muscovites from these dikes yielded the youngest ages (184 ± 1 and 180 ± 1 Ma, respectively). These ages are close to the $^{40}Ar/^{39}Ar$ date of muscovite of massive quartz–muscovite aggregate from the Molybdenum stock (Fig. 10).

The duration and mechanism of formation of the Kalguty OMS. New $^{40}Ar/^{39}Ar$ dates for the Kalguty OMS along with results of earlier geochronological studies (Berzina et al., 2003; Annikova et al., 2006; Seltmann et al., 2007; Gusev, 2011) point to the long-term formation of the Kalguty OMS as a whole (215–181 Ma) and the East Kalguty dike belt (202–181 Ma). Taking into account the geologic relations among various components of the Kalguty OMS, we have recognized five stages in its formation (Table 3, Fig. 10). The estimated ages should be correlated with the tectonic regime and magmatism in Gorny Altai. In the Early Mesozoic, this area underwent intraplate magmatism (Vladimirov et al., 1997, 2005; Shokal'skii et al., 2000; Annikova et al., 2006, 2014; Kruk, 2015).

At the intraplate stage of tectogenesis (MZ_1), the southern part of Gorny Altai underwent intense shear–pull-apart and normal–reverse fault dislocations, which formed an orthogonal grid of faults of NE and SE strikes (Fig. 1). An intense northeastward compression led to a repeated activity of the fault grid, which was expressed in shearing and reverse faulting. These dislocations were accompanied by the intrusion of granitoid magmas in the weakest zones at the points of intersection of faults. As a result, granite batholiths

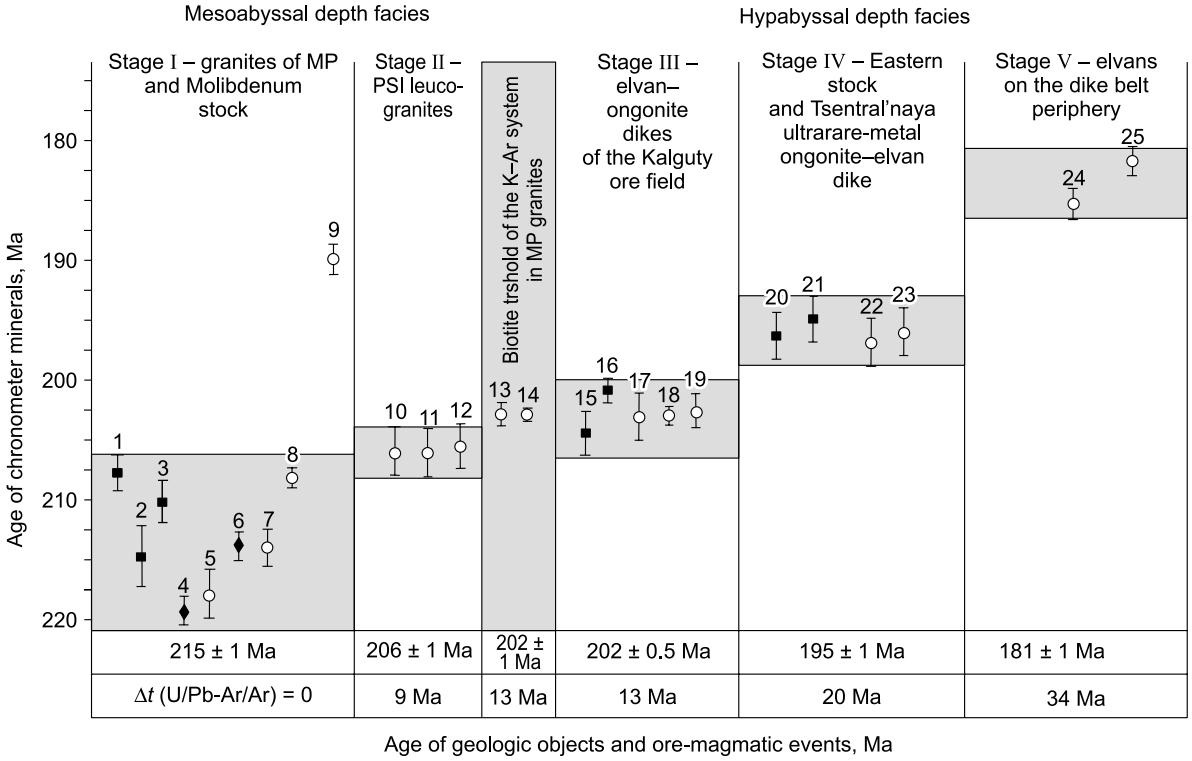

Fig. 10. Major temporal stages of formation of the Kalguty OMS. The numbers of dates follow Table 3; for explanation, see the text. Designations follow Fig. 9. PSI, Phase of supplementary intrusions; MP, major intrusive phase.

got to two magmatism areas, Bukhtarma and Kalguty. The U/Pb, Rb/Sr, and $^{40}Ar/^{39}Ar$ dating has shown the synchronous pulse formation of some magmatic rhythms and complexes within each area (245–230, 215–205, and 200–180 Ma), which reflects periodical tectonic activity in the region. However, the scales of granite formation, the mechanisms of melt intrusion, and the depths of melt occurrence were strongly different at the tectogenesis stages. This difference was best pronounced at the Early Jurassic stage of tectogenesis (205–180 Ma), when large mesoabyssal granitoid batholiths formed in the Bukhtarma magmatism area, whereas in the Kalguty area, where the large-scale granite formation had already ended, the tectonic rise of the granite batholith to the upper crustal horizons and the subsynchronous intrusion of subvolcanic ongonite and elvan dikes were the leading mechanism of tectogenesis. Thus, the intrusion and formation of the parental granitic magma of the Kalguty batholith occurred on the background of at least two phases of dislocations: 215–1010 Ma—the origin of a shear–normal-fault of NE strike, with the SE dip of the main shear plane of 60–70º, and 205–180 Ma—the activation of this shear–normal-fault to a shear–reverse-fault. Taking into account the geological, geophysical, and thermobarogeochemical data (Annikova et al., 2004; Sokolova et al., 2011a) and the results of the above thermochronological analysis, we suggest that the Kalguty OMS was a two-level magmatic column and the recently exposed Kalguty batholith was localized in the upper magma chamber, which formed at a much greater (mesoabyssal) depth (≥5–15 km) and then raised to a higher crustal level, $\Delta t \sim 5$ km (Fig. 11).

We performed a mathematical modeling to correlate the obtained geochronological ages with the duration of the cooling of one- and two-level magma columns in the crustal section.

MATHEMATICAL MODELING

Prerequisites. To study the dynamics of the cooling of interrelated magma chambers at different levels, we used a numerical-modeling algorithm with regard to a stationary crustal geotherm with an initial thermal gradient of 30 ºC/km (Spear, 1993; Polyansky et al., 2011) and to the general ther-

Table 5. Input parameters of the algorithm used for numerical modeling of the thermal history of the Kalguty OMS

Parameter	Intrusion	Host rocks
Thermal conductivity, W/(m·K)	4.01	3.48
Heat capacity, J/(kg·K)	693.35	733
Density, g/cm^3	2.6	2.93
Geothermal gradient, °C/km	—	30
Grid step, m	500	500
Liquidus temperature, °C	815	—
Solidus temperature, °C	815–600	—

Note. For explanation, see the text.

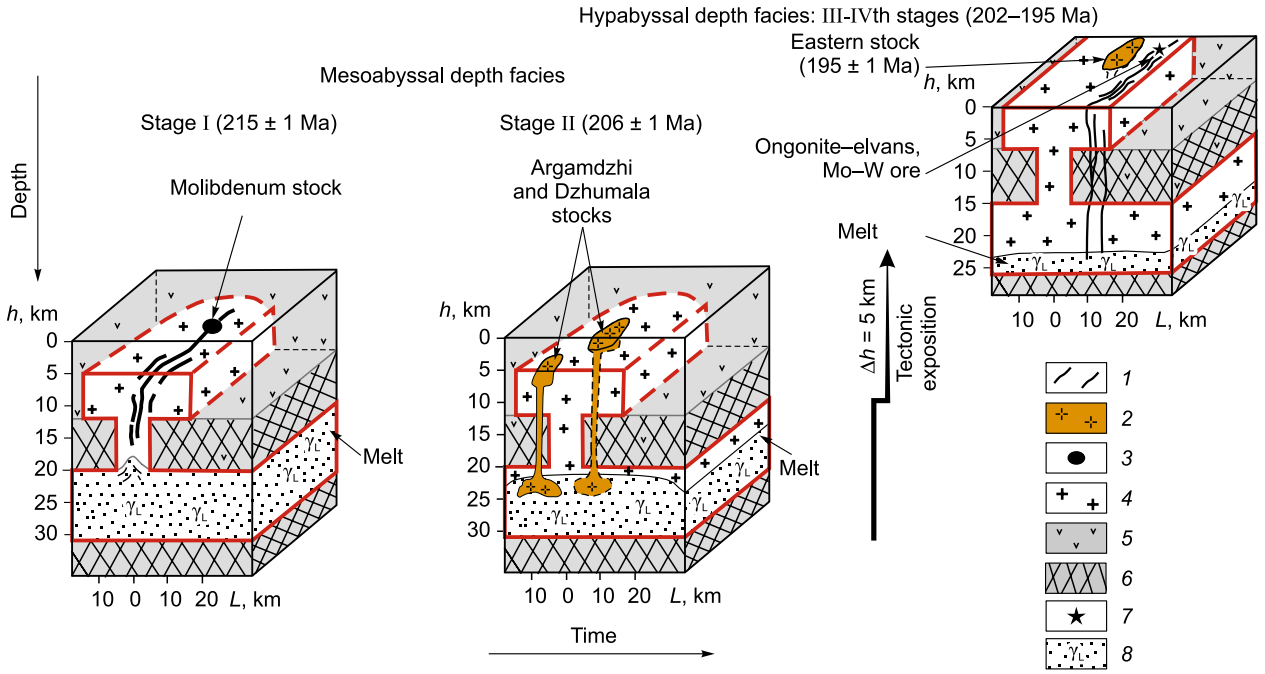

Fig. 11. Schematic model of the Kalguty OMS, depicting the successive cooling of the two-level magma column in the course of its tectonic rise (with the extension of the South Altai continental lithosphere) and shear–reverse-fault dislocations. *1*, ongonite–elvan dikes of the Mo–W deposit; *2*, undivided leucogranite stocks; *3*, Molybdenum stock; *4*, granites of major intrusive phase of the Kalguty batholith; *5*, volcanic rocks of the Aksai Formation (D_{1-2}); *6*, terrigenous rocks of the Gorny Altai Group (V–Є); *7*, Mo–W deposit; *8*, granite melt.

modynamic properties of granite formation (Murzintsev et al., 2016).

(1) The designed algorithm focuses on the reconstruction of the trends of granitic-magma cooling but ignores the problems of the mechanisms of melt genesis and intrusion, including: (a) the space problem, (b) granite–gneiss diapirism, (c) passive filling of local crustal decompression zones with granitic magma during the rheological crustal delamination, and (d) the role of contamination and mantle–crust interaction (mingling processes).

(2) The temperature gradient and thermal energy of fissionable elements in the crust are major factors, that is, the temperature distribution in the crust is determined by the stationary solution of the thermal-conductivity equation taking into account the content of fissionable elements in the crust and the temperature and temperature gradient at the Earth's surface (Spear, 1993; Polyansky et al., 2011). However, based on the properties of the haplogranite system Qtz–Ab–Or–H_2O, one should take into account that large-scale granite formation is governed by two factors: (1) pressure release and, as a result, decompression melting of the initial substratum and large-scale granite formation; (2) temperature increase due to the appearance of basic-magma chambers (underplating) at the mantle–crust boundary. It was shown earlier that both factors play a significant role in the formation of rare-metal granites and deposits in Gorny Altai (Vladimirov et al., 1997, 1998; Dobretsov et al., 2005; Annikova et al., 2006). However, the role of mantle sources in the formation of the Kalguty OMS is not taken into account (the reasoning is given above), and the large-scale taphrogenic extension of the continental lithosphere during shear–reverse-fault dislocations is reflected as the "instant rise" of the entire southern part of Gorny Altai (including the magma column) from the deep level (h ~ 5–30 km) to the upper crustal horizons ($h \leq$ 0–25 km).

(3) This algorithm also ignores the effect of chemical reactions on the P–T–X conditions of the haplogranite system. Therefore, the results obtained obviously correspond to conductive heat and mass transfer, when the "standard" granitic magma is in quasi-stationary conditions, i.e., in a closed system without external input of heat in the form of basic injections and(or) intratelluric mantle flows.

(4) The crystallization differentiation of granite melt, which was inevitable during the cooling of magma chambers, is taken into account as specified solidus temperatures at different crustal depths. The haplogranite system is characterized by the following solidus temperatures: ~730 ºC at 0.7 kbar, ~680 ºC at 2 kbar, ~660 ºC at 3 kbar, and ~645 ºC at 5 kbar (Johannes and Holtz, 1996).

The boundary conditions. The numerical modeling of the thermal history of formation of the Kalguty OMS was performed with regard to the physical properties of minerals and rocks (Tables 4 and 5).

(1) The morphology and deep structure of the Kalguty OMS (Fig. 3) are presented as the system upper magma chamber (granitoid batholith 6 km in thickness and 25 km in diameter)–feeding stem–deep-seated granite layer 11 km in

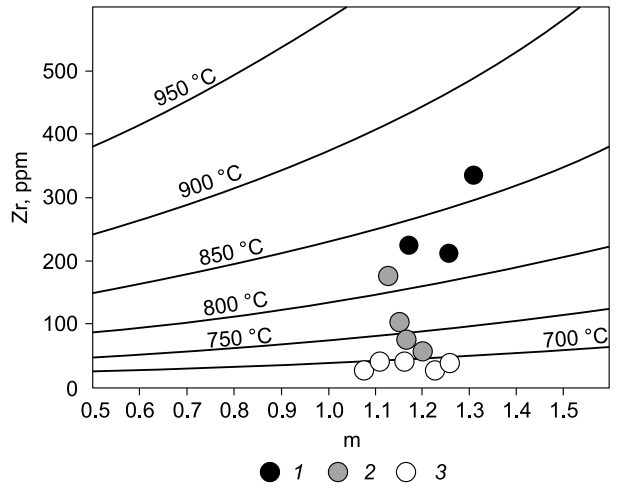

Fig. 12. Zr–M diagram for granitoids of the Kalguty pluton. Zircon saturation temperatures are shown by curves; M = (Na + K + 2Ca)/(Al·Si) (the amounts of elements are taken in molar fractions) (Watson and Harrison, 1983). *1*, stage I of the Kalguty OMS—major-phase granites; *2*, stage II of the Kalguty OMS—leucogranites of the Dzhumala and Argamdzha stocks; *3*, stages IV and V of the Kalguty OMS—ongonite–elvans of the East Kalguty dike belt.

thickness. The latter layer was, most likely, closely related to the magma-forming substratum.

(2) The age boundaries of the formation of the Kalguty OMS are shown in Fig. 10. The extension of the continental lithosphere ("biotite threshold", "instant decompression") is taken in the algorithm as the mechanical transfer of a magma column from deep to upper crustal level.

(3) The Early Paleozoic graywackes of the Gorny Altai volcanosedimentary series were taken as a protolith (Shokal'skii et al., 2000; Kruk, 2015). The normative mineral composition of the graywackes of the Gorny Altai terrigenous strata is as follows (%): quartz—10, plagioclase—50, and augite—40.

(4) The composition of the parental magma apparently corresponded to the granites of major intrusive phase (Table 1). The averaged normative mineral composition of major-phase granites of the Kalguty batholith is as follows (%): quartz—30, plagioclase—35, and K-feldspar—35.

(5) The thermal regime of the Kalguty OMS was evaluated with the Zr thermometer (Watson and Harrison, 1983; Boehnke et al., 2013). According to the calculations (Fig. 12), the biotite granites of major intrusive phase are the highest-temperature rocks of the Kalguty OMS (857–815 ºC, the average over three analyses is 835 ºC), the leucogranites of the supplementary intrusive phase are characterized by wide temperature variations, 812–701 ºC (the average over four analyses is 750 ºC), and the ongonites of the final phase are the lowest-temperature rocks, 693–652 ºC (the average over five analyses is 674 ºC). These data are consistent with the general homodromous trend of the Kalguty OMS (the temperatures decrease from biotite granites via leucogranites to ongonites), which corresponds to the recognized intrusive phases. Therefore, a temperature of 815 ºC is taken as the liquidus temperature of the parental granitic magma.

(6) The solidus temperature of the residual granite melt was taken equal to 600–630 ºC (depending on the depth of crystallization), based on the results of thermobarogeochemical study of melt inclusions in ongonites and elvans of the East Kalguty dike belt (Sokolova et al., 2011a).

Discussion of the numerical-modeling results. The calculation results show that 10 Myr after the intrusion of major phase, a melt stays at depths of more than 25 km for a long time (≥20 Myr). This is due to the fact that the upper magma chamber and the feeder are rapidly frozen and the existence of the melt is governed only by the equilibrium temperature in the horizon, which, in turn, is determined by the stationary geotherm. That is, at depths of less than 25 km, the feeder, like the pluton itself, is completely consolidated for 2.2 Myr and its temperature becomes equal to the ambient temperature, whereas at depths of more than 25 km, the ambient temperature determined by the stationary geotherm becomes higher than the solidus temperature of the granite melt and its residual portions can be preserved in the liquid state for tens to hundreds of Myr. This theoretical conclusion is correct only for a "quiet" geodynamic setting, without tectonic dislocations (Travin et al., 2009; Travin, 2016). The appearance of an "external" tectonic factor (e.g., rise of a geoblock) becomes decisive for the cooling of a granitoid batholith. The calculations for a two-level magma column, most similar to that of the Kalguty OMS (Figs. 11 and 13), show that the melt evolves for 12 Myr after its intrusion; after the rise of the entire geoblock (including the magma column) by 5 km, the residual rare-metal melt continues evolving in a deep-seated magma chamber for 20 Myr since the beginning of the formation of the Kalguty OMS (Fig. 13). This scenario permits estimation of the temporal stages and duration of the formation of the Kalguty OMS, including the East Kalguty ongonite–elvan dike complex and the spatially and temporally associated Mo–W quartz-vein–greisen deposit.

CONCLUSIONS

(1) The thermochronological analysis of igneous rocks and ores composing the Kalguty OMS made it possible to recognize five stages in its formation: I (215 ± 1 Ma)—formation of granites of major intrusive phase and of Mo-rich mineralization, which is an orebody called the Molybdenum stock; II (206 ± 1 Ma)—formation of leucogranite and intragranitic-pegmatite stocks in granites of major intrusive phase; III (202 ± 1 Ma)—formation of most of ongonite–elvan dikes composing a dike belt; IV (195 ± 1 Ma)—formation of long ultrarare-metal ongonite–elvan dikes in the central part of the dike belt, which is spatially associated with the W-rich veins of the deposit; and V (181 ± 1 Ma)—formation of thin ongonite–elvan dikes on the periphery of the

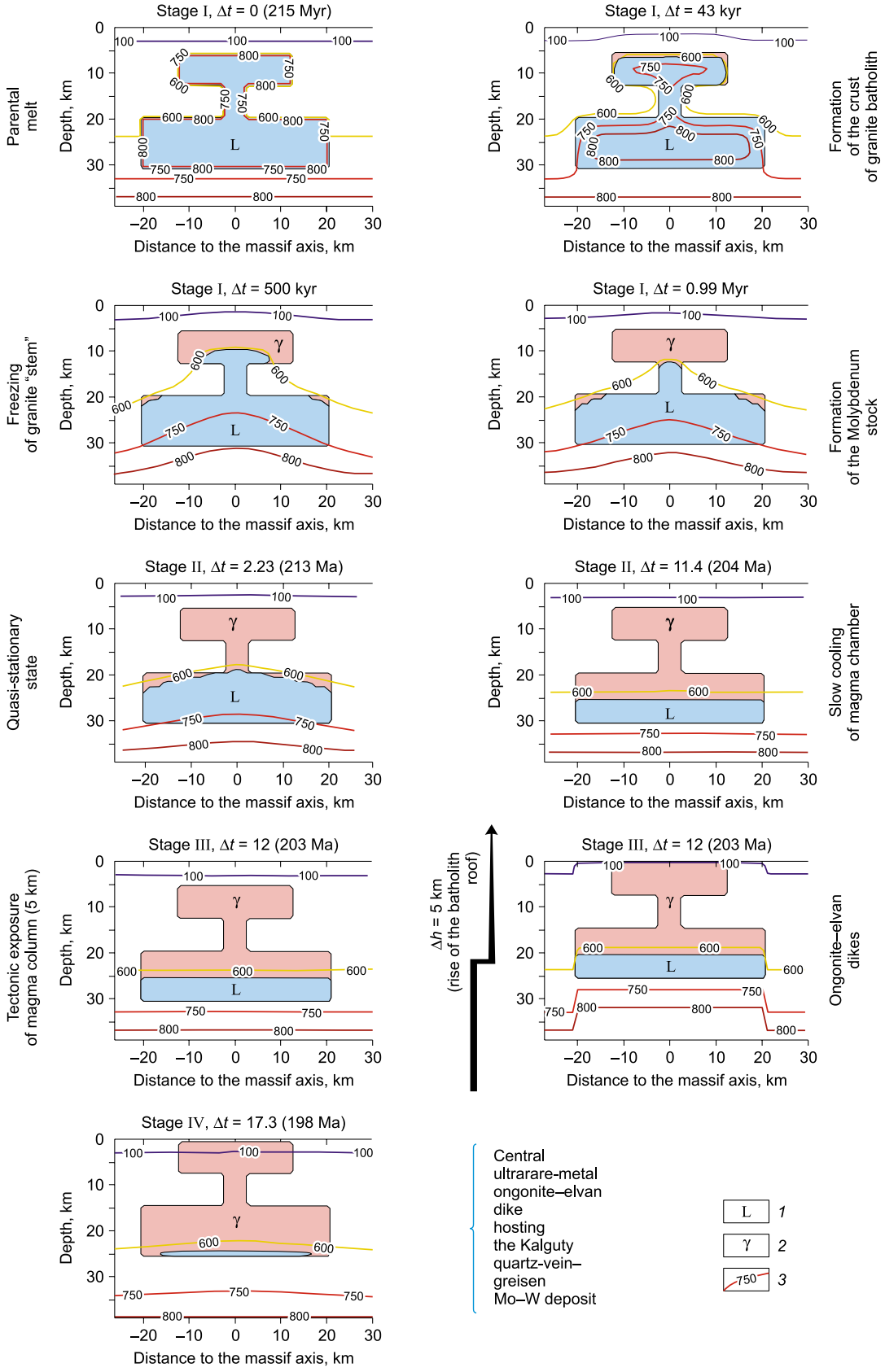

Fig. 13. Results of numerical modeling showing the dynamics of cooling of the Kalguty OMS in the crustal section. The two-level model implies granitoid batholith–feeder–magma chamber, $\Delta t = t_{1(U/Pb)} - t_{2\ (Ar/Ar)}$). For other explanation, see the text. *1*, granite melt; *2*, crystalline granite; *3*, isotherm (ºC).

dike belt. The total duration of the ore-magmatic processes is 20 Myr (Mo–W ore-productive stage) or 30 Myr, if taking into account occasional elvan dikes on the periphery of the Kalguty deposit, which are spatially associated with quartz–fluorite–barite–ferberite veins (181 ± 1 Ma).

(2) The mathematical modeling of the thermal history of the Kalguty OMS shows that the formation of a granite batholith (215 ± 1 Ma) and a later ongonite–elvan dike complex with Mo–W-rich mineralization (195 ± 1 Ma) can be explained by a two-level magma column with the "upper" granite batholith at a depth of 5–15 km and the "lower" granite chamber at a depth of 20–31 km, which are connected by a granite stem (feeder).

(3) The decisive factor that determined the thermal cooling of the Kalguty OMS was the tectonic rise of the entire magma column to the upper crustal horizons. Only in this case does the solution of the inverse physical problem ensure correlation between the thermochronological data and the results of numerical modeling.

We are sincerely grateful to Dr. A.S. Borisenko, Dr. N.N. Kruk, and Dr. V.A. Ponomarchuk for the long-term discussion of the considered problems.. We also thank Dr. G.G. Pavlova, Dr. A.N. Berzina, Dr. D.S. Yudin, Dr. S.V. Khromykh, Dr. P.D. Kotler, and Dr. S.A. Vystavnoi for participation in the joint expeditionary research and provision of their results of geochronological studies. We must emphasize the great contribution of Dr. A.A. Obolensky, Dr. A.V. Titov, and Dr. V.B. Dergachev to the study of the Kalguty OMS; this paper would be impossible without their research materials. Special thanks to O.P. Gerasimov for expeditionary work, I.A. Vladimirov for GIS technology, and T.V. Miryasova and O. Yu. Dubrovin for the paper design.

The work was performed in the framework of the state task from the Institute of Geology and Mineralogy, Novosibirsk, with the financial support by the Ministry of Education and Science of the Russian Federation (projects 5.1688.2017/PCh (numerical modeling of the Kalguty OMS) and 14.Y26.31.0012 (designing of computer graphics and construction of a petrological model of the Kalguty OMS)) and by the Russian Foundation for Basic Research (grants 16-05-00128a (^{40}Ar/^{39}Ar isotope studies of rocks and ores of the Kalguty OMS), 17-05-00936a (interpretation of geochronological research data and thermochronological analysis), and 17-55-540001 (processing of fond materials)).

REFERENCES

Alekseev, V.I., 2013. The Far East province of rare-metal–Li–F granites and its ore potential, in: Problems of Mineralogy, Petrography, and Metallogeny. P.N. Chirvinskii Commemorative Scientific Readings [in Russian]. Izd. PGNIU, Perm', No. 16, 258–263.

Amshinskii, N.N., 1973. Vertical Petrogeochemical Zonation of Granitoid Plutons [in Russian]. Zapadno-Sibirskoe Knizhnoe Izdatel'stvo, Novosibirsk.

Annikova, I.Yu., Vladimirov, A.G., Vystavnoi, S.A., Vasilevsky, A.N., Vitte, L.V., Moroz, E.N., 2004. Geological and geophysical model of formation of the Kalguty ore-magmatic system (southern Altai). Izvestiya TPU 307 (4), 38–42.

Annikova, I.Yu., Vladimirov, A.G., Vystavnoi, S.A., Zhuravlev, D.Z., Kruk, N.N., Lepekhina, E.N., Matukov, D.I., Moroz, E.N., Palesskii, S.V., Ponomarchuk, V.A., Rudnev, S.N., Sergeev, S.A., 2006. U–Pb and ^{39}Ar/^{40}Ar dating and Sm–Nd and Pb–Pb isotopic study of the Kalguty molybdenum–tungsten ore-magmatic system, southern Altai. Petrology 14 (1), 81–97.

Annikova, I.Yu., Borisenko, A.S., Borovikov, A.A., Goverdovskiy, V.A., Kruk, N.N., Naumov, E.A., Obolenskiy, A.A., Pavlova, G.G., Travin, A.V., Tretyakova, I.G., Vladimirov, A.G., 2007. The South-Chuya Ridge and the Ukok Plateau (southern part of Gorny Altai), in: Metallogeny of the Southern Altai (Russia) and Northwestern Mongolia Ore District, Permian–Triassic Boundary. Guidebook of Field Excursion, London, Novosibirsk, pp. 63–77.

Annikova, I.Yu., Smirnov, S.Z., Sokolova, E.N., Khromykh, S.V., Vladimirov, A.G., Travin, A.V., 2014. Evolution of magma chamber during the formation of the East Kalguty rare-metal granitoid dike belt (Gorny Altai), in: Proceedings of the Second International Geological Conference "Granites and the Earth's Evolution", Novosibirsk, 17–20 August 2014 [in Russian]. Izd. SO RAN, Novosibirsk, pp. 15–19.

Antipin, V.S., Savina, E.A., Mitichkin, M.A., Perelyaev, V.I., 1999. Rare-metal–Li–F granites, ongonites, and topazites of the southern Baikal area. Petrologiya 7 (2), 141–155.

Antipin, V.S., Halls, C., Mitichkin, M.A., Scott, P., Kuznetsov, A.N., 2002. Elvans of Cornwall (England) and southern Siberia as subvolcanic counterparts of subalkalic rare metal granites. Geologiya i Geofizika (Russian Geology and Geophysics) 43 (9), 847–857 (798–807).

Antipin, V.S., Andreeva, I.A., Kovalenko, V.I., Kuznetsov, V.A., 2009. Geochemical specifics of ongonites in the Ary-Bulak massif, eastern Transbaikalia. Petrology 17 (6), 558–569.

Antipin, V.S., Perepelov, A.B., Ochir, G., Odgerel, D., Tsegmed, Z., 2016. Late Paleozoic and Early Mesozoic rare-metal granites in Central Mongolia and Baikal region: review of geochemistry, possible magma sources and related mineralization. J. Geosci. 61, 105–125.

Averkin, Yu.A., Cherepanov, A.N., Sharapov, V.N., 1988. Evolution of Fluid Systems under Retrograde Boiling of Magmas [in Russian]. IGiG SO AN SSSR, Novosibirsk (preprint).

Badanina, E.V., Syritso, L.F., Volkova, E.V., Thomas, R., Trumbull, R.B., 2010. Composition of Li–F granite melt and its evolution during the formation of the ore-bearing Orlovka massif in eastern Transbaikalia. Petrology 18 (2), 131–157.

Baksi, A.K., Archibald, D.A., Farrar, E., 1996. Intercalibration of ^{40}Ar/^{39}Ar dating standards. Chem. Geol. 129, 307–324.

Berzina, A.N., Stein, H.J., Zimmerman, A., Sotnikov, V.I., 2003. Re–Os ages for molybdenite from porphyry Cu–Mo and greisen Mo–W deposits of southern Siberia (Russia) preserve metallogenic record, in: Mineral Exploration and Sustainable Development. Millpress, Rotterdam, p. 213.

Black, L.P., Kamo, S.L., 2003. TEMORA 1: a new zircon standard for U–Pb geochronology. Chem. Geol. 200, 155–170.

Boehnke, P., Watson, E.B., Trail, D., Harrison, T.M., Schmitt, A.K., 2013. Zircon saturation re-revisited. Chem. Geol. 351, 324–334.

Cobbing, E.J., Mallick, D.I., Pitfield, P.E., Teoh, L.H., 1986. The granites of the Southeast Asian Tin Belt. J. Geol. Soc. London 143, 537–550.

D'yachkov, B.A., 2012. Genetic Types of Rare-Metal Deposits in the Kalba–Narym Belt [in Russian]. VKGTU, Ust'-Kamenogorsk.

Darbyshire, D.P.F., Shepherd, T.J., 1994. Nd and Sr isotope constraints on the origin of the Cornubian batholith, SW England. J. Geol. Soc. London 151, 795–802.

Dergachev, V.B., 1988. A new variety of ongonites. Dokl. Akad. Nauk SSSR 302 (1), 188–191.

Dergachev, V.B., 1989a. Regularities of formation of rare-metal granite dikes, in: Prediction of Rare-Metal and Gold Mineralization in the Altai–Sayan Folded Area [in Russian]. SNIIGGiMS, Novosibirsk, pp. 60–70.

Dergachev, V.B., 1989b. Cesium variety of ultrarare-metal granite porphyry (elvans). Dokl. Akad. Nauk SSSR 305 (6), 708–712.

Dergachev, V.B., Timofeev, N.I., Ladygina, I.N., 1981. Zonation of the Kalguty Mo–W deposit, in: Zonation of Ore Deposits in Siberia [in Russian]. SNIIGGiMS, Novosibirsk, Issue 289, pp. 84–92.

Dobretsov, N.L., Vladimirov, A.G., Kruk, N.N., 2005. Permian–Triassic magmatism in the Altai–Sayan fold system as a reflection of the Siberian superplume. Dokl. Earth Sci. 400 (1), 40–43.

Dobretsov, N.L., Borisenko, A.S., Izokh, A.E., Zhmodik, S.M., 2010. A thermochemical model of Eurasian Permo–Triassic mantle plumes as a basis for prediction and exploration for Cu–Ni–PGE and rare-metal ore deposits. Russian Geology and Geophysics (Geologiya i Geofizika) 51 (9), 903–924 (159–1187).

Dortman, N.B. (Ed.), 1984. Physical Properties of Rocks and Minerals (Petrophysics). Guide to Geophysics [in Russian]. Nedra, Moscow.

Fleck, R.J., Sutter, J.F., Elliot, D.H., 1977. Interpretation of discordant $^{40}Ar/^{39}Ar$ age-spectra of Mesozoic tholeiites from Antarctica. Geochim. Cosmochim. Acta 41, 15–32.

Gonevchuk, V.G., 2002. Tin-Bearing Systems in the Far East: Magmatism and Ore Genesis [in Russian]. Dal'nauka, Vladivostok.

Gusev, N.I., 2011. Chronology (SHRIMP II) of magmatism in the Kalguty rare-metal–tungsten–molybdenum ore–magmatic system, Gorny Altai, Russia. Geol. Ore Deposits 53 (3), 248–263.

Johannes, W., Holtz, F., 1996. Petrogenesis and Experimental Petrology of Granitic Rocks. Springer, Berlin, New York, p. 335.

Kostitsyn, Yu.A., Zaraiskii, G.P., Aksyuk, A.M., Chevychelov, V.Yu., 2004. Rb–Sr evidence for the genetic links between biotite and Li–F granites: an example of the Spokoinoe, Orlovka, and Etyka deposits, eastern Transbaikalia. Geochem. Int. 42 (9), 822–829.

Kovalenko, V.I., Kovalenko, N.I., 1976. Ongonites (Topaz-Containing Quartz Keratophyres), Subvolcanic Analogs of Rare-Metal–Li–F Granites [in Russian]. Nauka, Moscow.

Kovalenko, V.I., Kostitsyn, Yu.A., Yarmolyuk, V.V., Budnikov, S.V., Kovach, V.P., Kotov, A.B., Sal'nikova, E.B., Antipin, V.S., 1999. Sources of magmas and isotope (Sr, Nd) evolution of rare-metal–Li–F granitoids. Petrologiya 7 (4), 401–429.

Kretz, R., 1983. Symbols for rock-forming mineral. Am. Mineral. 68, 277–279.

Kruk, N.N., 2015. Continental crust of Gorny Altai: stages of formation and evolution; indicative role of granitoids. Russian Geology and Geophysics (Geologiya i Geofizika) 56 (8), 1097–1113 (1403–1423).

Kuz'min, M.I., Yarmolyuk, V.V., 2011. Plumes and associated mineral deposits, in: The Modern State of Geosciences. Proceedings of Scientific and Practical Conference [in Russian]. Izd. MGU, Moscow, pp. 1032–1034.

Merceron, T., Vieillard, P., Fouillac, A.M., Meunier, A., 1992. Hydrothermal alterations in the Echassières granitic cupola (Massif Central, France). Contrib. Mineral. Petrol. 112 (2), 279–292.

Morozova, I.M., Rublev, A.G., 1987. K–Ar systems of polymetamorphic rocks, in: Shukolyukov, Yu.A. (Ed.), Isotope Dating of Metamorphism and Metasomatism Processes [in Russian]. Nauka, Moscow, pp. 19–28.

Murzintsev, N.G., Travin, A.V., Kotler, P.D., Vladimirov, A.G., 2016. Numerical modeling of the thermal history and the area of the thermal effect of a granite massif on the host rocks and of the behavior of the K–Ar system in geochronometer minerals, in: Petrology of Igneous and Metamorphic Formations. Issue 8. Proceedings of All-Russian Petrographic Conference with International Participation [in Russian]. Izd. Tomskogo TsNTI, Tomsk, pp. 256–259.

Oitseva, T.A., Kuzmina, O.N., Murzintsev, N.G., Kotler, P.D., 2016. Rare metal structures, mineral types and age of the pegmatite deposits of Qalba–Narym granitoid belt, in: Proceedings of the 8th International Siberian Early Career Geoscientists Conference, Novosibirsk, 13–24 June 2016. IGM SB RAS, IPPG SB RAS, NSU, pp. 216–217.

Polyansky, O.P., Sukhorukov, V.P., Travin, A.V., Alekhin, I.G., Yudin, D.S., 2011. Tectonic interpretation of the thermochronological data and *PT*-conditions of rock metamorphism in the Bodonchin zonal complex (Mongolian Altay). Russian Geology and Geophysics (Geologiya i Geofizika) 52 (9), 991–1006 (1256–1275).

Potseluev, A.A., Rikhvanov, L.P., Vladimirov, A.G., Annikova, I.Yu., Babkin, D.I., Nikiforov, A.Yu., Kotegov, V.I., 2008. The Kalguty Rare-Metal Deposit (Gorny Altai): Magmatism and Ore Genesis [in Russian]. STT, Tomsk.

Raimbault, L., Cuney, M., Azencott, C., Duthou, J.L., Joron, J.L., 1995. Geochemical evidence for a multistage magmatic genesis of Ta–Sn–Li mineralization in the granite at Beauvoir, French Massif Central. Econ. Geol. 90, 548–576.

Rub, A.K., Rub, M.G., 2006. Rare-Metal Granites in Primorye [in Russian]. VIMS, Moscow.

Seltmann, R., Borisenko, A., Fedoseev, G. (Eds.), 2007. Magmatism and Metallogeny of the Altai and Adjacent Large Igneous Provinces with an Introductory Essay on the Altaids. IAGOD Guidebook Series 16, CERCAMS/NHM, London.

Shanin, L.L., 1979. Criteria for reliability and possible causes of distortion of radiological dates, in: Criteria for the Reliability of Radiological Dating Methods [in Russian]. Nauka, Moscow, pp. 6–13.

Sharapov, V.N., Averkin, Yu.A., 1990. Dynamics of Heat and Mass Exchange in Orthomagmatic Fluid Systems [in Russian]. Nauka, Novosibirsk.

Shcherba, G.N., D'yachkov, B.A., Stuchevskii, N.I., Nakhtigal', G.P., Antonenko, A.N., Lyubetskii, V.N., 1998. The Greater Altai (Geology and Metallogeny). Book 1. Geologic Structure [in Russian]. Gylym, Almaty.

Shcherba, G.N., Bespaev, Kh.A., D'yachkov, B.A., Mysnik, A.M., Ganzhenko, G.D., Sapargaliev, E.M., 2000. The Greater Altai (Geology and Metallogeny). Book 2. Metallogeny [in Russian]. RIO VAK RK, Almaty.

Shokal'skii, S.P., Babin, G.A., Vladimirov, A.G., Borisov, S.M., Gusev, N.I., Tokarev, V.N., Zybin, V.A., Dubskii, V.S., Murzin, O.V., Krivchikov, V.A., Kruk, N.N., Rudnev, S.N., Fedoseev, G.S., Titov, A.V., Sergeev, V.P., Likhachev, N.N., Mallin, A.N., Kotel'nikov, E.I., Kuznetsov, S.A., Zeifert, L.L., Yashin, V.D., Noskov, Yu.S., Uvarov, A.N., Fedak, S.I., Gusev, A.I., Vystavnoi, S.A., 2000. Correlation between Igneous and Metamorphic Complexes in the West of the Altai–Sayan Folded Area [in Russian]. Izd, SO RAN, Filial "Geo", Novosibirsk.

Sokolova, E.N., Smirnov, S.Z., Astrelina, E.I., Annikova, I.Yu., Vladimirov, A.G., Kotler, P.D., 2011a. Ongonite–elvan magmas of the Kalguty ore-magmatic system (Gorny Altai): composition, fluid regime, and genesis. Russian Geology and Geophysics (Geologiya i Geofizika) 52 (11), 1378–1400 (1748–1775).

Sokolova, E., Smirnov, S., Annikova, I., 2011b. Compositions of magmatic melts at formation of chemically heterogeneous rare-metal felsic dike in the East Kalguty dike belt (Gorny Altay, Russia), in: European Current Research on Fluid Inclusions. Abstracts of the 21st Biennial Conference, Leoben, Austria, 9–11 August 2011. Geologische Bundesanstalt, Vienna, pp. 174–175.

Spear, F.S., 1993. Metamorphic phase equilibria and pressure–temperature–time paths. Mineral. Soc. Am., Washington, D.C.

Štemprok, M., Pivec, E., Langrová, A., 2005. The petrogenesis of a wolframite-bearing greisen in the Vykmanov granite stock, Western Krušné hory pluton (Czech Republic). Bull. Geosci. 80 (3), 163–184.

Titov, A.V., Vladimirov, A.G., Vystavnoi, S.A., Pospelova, L.N., 2001. Extraordinary high-temperature felsite porphyries in the postgranite dike swarm of the Kalguty rare-metal granite massif, Gornyi Altai Mountains. Geochem. Int. 39 (6), 615–620.

Travin, A.V., 2016. Thermochronology of Early Paleozoic collisional and subduction-collisional structures of Central Asia. Russian Geology and Geophysics (Geologiya i Geofizika) 57 (3), 434–450 (553–574).

Travin, A.V., Yusin, D.S., Vladimirov, A.G., Khromykh, S.V., Volkova, N.I., Mekhonoshin, A.S., Kolotilina, T.B., 2009. Thermochronology of the Chernorud granulite zone, Ol'khon region, western Baikal area. Geochem. Int. 47 (11), 1107–1124.

Vasilevskii, A.N., 1980. Use of the trial and error method in modeling regional geologic structures. Geologiya i Geofizika (Soviet Geology and Geophysics) 21 (3), 83–93 (67–74).

Vinogradov, A.P., 1962. Average contents of chemical elements in the main types of igneous crustal rocks. Geokhimiya, No. 7, 555–571.

Vitte, L.V., 1981. Types of Continental Earth's Crust and Their Evolution [in Russian]. Nauka, Novosibirsk.

Vitte, L.V., Vasilevskii, A.N., 1988. The question of tectonic position and forms of manifestations of alkaline ultrabasic magmatism in the crust of the Siberian Platform. Geologiya i Geofizika (Soviet Geology and Geophysics 29 (5), 55–65 (46–54).

Vladimirov, A.G., Kruk, N.N., Chupin, V.P., Turkina, O.M., Rudnev, S.N., Vladimirov, V.G., Titov, A.V., 1991. Topaz–protolithionite granites and ongonites of the Bazardara ore formation (northeastern Russia). Geologiya i Geofizika (Soviet Geology and Geophysics) 32 (4), 40–48 (34–41).

Vladimirov, A.G., Chupin, V.P., Kruk, N.N., Averkin, Yu.A., 1993. Dynamics of crystallization of multiphase leucogranite massifs and the problem of residual Li–F-magma chambers (by the example of the Bazarda massif, southeastern Pamir). Dokl. Akad. Nauk 328 (1), 82–83.

Vladimirov, A.G., Ponomareva, A.P., Shokalskii, S.P., Khalilov, V.A., Kostitsyn, Yu.A., Ponomarchuk, V.A., Rudnev, S.N., Vystavnoi, S.A., Kruk, N.N., Titov, A.V., 1997. Late Paleozoic–Early Mesozoic granitoid magmatism in Altai. Geologiya i Geofizika (Russian Geology and Geophysics) 38 (4), 715–729 (755–770).

Vladimirov, A.G., Vystavnoi, S.A., Titov, A.V., Rudnev, S.N., Dergachev, V.B., Annikova, I.Yu., Tikunov, Yu.V., 1998. Petrology of Early Mesozoic rare-metal granites of Southern Gorny Altai. Geologiya i Geofizika (Russian Geology and Geophysics) 39 (7), 901–916 (909–924).

Vladimirov, A.G., Kruk, N.N., Rudnev, S.N., Khromykh, S.V., 2003. Geodynamics and granitoid magmatism of collisional orogens. Geologiya i Geofizika (Russian Geology and Geophysics) 44 (12), 1321–1338 (1275–1292).

Vladimirov, A.G., Kruk, N.N., Polyansky, O.P., Vladimirov, V.G., Babin, G.A., Rudnev, S.N., Annikova, I.Yu., Travin, A.V., Savinykh, Ya.V., Palesskii, S.V., 2005. Correlation among Hercynian dislocations, sedimentation, and magmatism in the Altai collisional system as a reflection of plate and plume tectonics, in: Geodynamic Evolution of the Lithosphere in the Central Asian Mobile Belt (from Ocean to Continent) [in Russian]. GIN RAN, Moscow, pp. 182–215.

Vladimirov, A.G., Kruk, N.N., Khromykh, S.V., Polyansky, O.P., Chervov, V.V., Vladimirov, V.G., Travin, A.V., Babin, G.A., Kuibida, M.L., Khomyakov, V.D., 2008. Permian magmatism and lithospheric deformation in the Altai caused by crustal and mantle thermal processes. Russian Geology and Geophysics (Geologiya i Geofizika) 49 (7), 468–479 (621–636).

Vladimirov, A.G., Lyakhov, N.Z., Zagorskiy, V.E., Makagon, V.M., Kuznetsova, L.G., Smirnov, S.Z., Isupov, V.P., Belozerov, I.M., Uvarov, A.N., Gusev, G.S., Yusupov, T.S., Annikova, I.Yu., Beskin, S.M., Shokal'skiy, S.P., Mikheev, E.I., Kotler, P.D., Moroz, E.N., Gavryushkina, O.A., 2012a. Lithium deposits of spodumene pegmatites in Siberia. Chemistry for Sustainable Development 20 (1), 3–20.

Vladimirov, A.G., Phan Luu Anh, Kruk, N.N., Smirnov, S.Z., Annikova, I.Yu., Pavlova, G.G., Kuibida, M.L., Moroz, E.N., Sokolova, E.N., Astrelina, E.I., 2012b. Petrology of the tin-bearing granite–leucogranites of the Piaoak Massif, Northern Vietnam. Petrology 20 (6), 545–566.

Watson, E.B., Harrison, T.M., 1983. Zircon saturation revisited: temperature and composition effects in a variety of crustal magma types. Earth Planet. Sci. Lett. 64, 295–304.

Williams, I.S., 1998. U–Th–Pb geochronology by ion microprobe, in: McKibben, M.A., Shanks III, W.C., Ridley, W.I., Applications of Microanalytical Techniques to Understanding Mineralizing Processes. Rev. Econ. Geol. 7, 1–35.

Zen, E., 1986. Aluminum enrichment in silicate melts by fractional crystallization: some mineralogic and petrographic constraints. J. Petrol. 27, 1095–1117.

Zagorsky, V.Ye., Vladimirov, A.G., Makagon, V.M., Kuznetsova, L.G., Smirnov, S.Z., D'yachkov, B.A., Annikova, I.Yu., Shokalsky, S.P., Uvarov, A.N., 2014. Large fields of spodumene pegmatites in the settings of rifting and postcollisional shear–pull-apart dislocations of continental lithosphere. Russian Geology and Geophysics (Geologiya i Geofizika) 55 (2), 237–251 (303–322).

Editorial responsibility: O.P. Polyansky